Stem Cell Reports
Article
ISSCR
OPEN ACCESS

ANXA3/JNK Signaling Promotes Self-Renewal and Tumor Growth, and Its Blockade Provides a Therapeutic Target for Hepatocellular Carcinoma

Man Tong,[1] Tsun-Ming Fung,[1] Steve T. Luk,[1] Kai-Yu Ng,[1] Terence K. Lee,[2,6] Chi-Ho Lin,[7] Judy W. Yam,[2,6] Kwok Wah Chan,[2] Fai Ng,[3] Bo-Jian Zheng,[3] Yun-Fei Yuan,[8] Dan Xie,[8] Chung-Mau Lo,[4,6] Kwan Man,[4,6] Xin-Yuan Guan,[5,6] and Stephanie Ma[1,6,*]

[1]Department of Anatomy
[2]Department of Pathology
[3]Department of Microbiology
[4]Department of Surgery
[5]Department of Clinical Oncology
[6]State Key Laboratory for Liver Research
[7]Centre for Genomic Sciences
Li Ka Shing Faculty of Medicine, The University of Hong Kong, Hong Kong
[8]State Key Laboratory of Oncology in Southern China, Sun Yat-Sen University Cancer Center, Guangzhou, China
*Correspondence: stefma@hku.hk
http://dx.doi.org/10.1016/j.stemcr.2015.05.013

SUMMARY

Frequent tumor relapse in hepatocellular carcinoma (HCC) has been commonly attributed to the presence of residual cancer stem cells (CSCs) after conventional treatments. We have previously identified and characterized CD133 to mark a specific CSC subset in HCC. In the present study, we found endogenous and secretory annexin A3 (ANXA3) to play pivotal roles in promoting cancer and stem cell-like features in $CD133^+$ liver CSCs through a dysregulated JNK pathway. Blockade of ANXA3 with an anti-ANXA3 monoclonal antibody in vitro as well as in human HCC xenograft models resulted in a significant reduction in tumor growth and self-renewal. Clinically, ANXA3 expression in HCC patient sera closely associated with aggressive clinical features. Our results suggest that ANXA3 can serve as a novel diagnostic biomarker and that the inhibition of ANXA3 may be a viable therapeutic option for the treatment of $CD133^+$ liver-CSC-driven HCC.

INTRODUCTION

Hepatocellular carcinoma (HCC) is the most common form of liver cancer. Resection and liver transplantation is remedial for early-stage HCC. Yet, since most patients are diagnosed at an advanced stage, therapy is rarely curative and the prognosis for the disease is poor. Despite advances in diagnosis and treatment, the disease remains a major health concern due to the infiltrative nature of these tumors, their resistance to chemotherapy, their high rate of recurrence, and our limited understanding of the mechanisms underlying initiation and progression of the disease. This dismal situation motivates the search for new therapies and better diagnostic biomarkers for detection of the disease at an earlier stage.

The cancer stem cell (CSC) model has helped explain why tumor eradication has not been achieved despite advances in treatment. The model suggests that a cellular hierarchy exists in some cancers, with self-renewing CSCs generating progeny constituting the tumor bulk. CSCs possess both tumor and stem cell-like properties (Pardal et al., 2003). Studies have shown that CSCs bear the exclusive ability to regenerate tumors. Treatment of bulk cancer cell populations within tumors with chemotherapy has been shown to select for the outgrowth of therapy-resistant cancer cells that are more tumorigenic, invasive, and stem-like. Hence, cancer therapies may be rendered ineffective because the bulk of cancer cells within a tumor may be eliminated while leaving behind CSC-enriched cells that proceed to regenerate tumors. This underscores the need for a detailed understanding of the molecular differences between CSCs and non-CSCs to discover cell-state-specific features that may render CSCs susceptible to selective therapeutic intervention.

The perpetuation of many cancer types has been suggested to stem from CSCs. We have found HCC to be driven by a liver CSC subset marked by the CD133 phenotype. $CD133^+$ HCC cells display sustained self-renewal, differentiate toward multiple lineages, and phenocopy the original tumor upon xenotransplantation (Ma et al., 2007, 2010). These cells also possess an enhanced ability to resist chemotherapy through activated AKT/BCL-2 (Ma et al., 2008). CD133 is not simply a marker of liver CSCs; it also plays a functional role in regulating HCC tumorigenesis (Tang et al., 2012). Increased CD133 expression in HCC is associated with worse overall survival and higher recurrence rates (Ma et al., 2010). Our results are consistent with studies by other groups where CD133 was also found to be an important risk factor for overall survival of the disease, demonstrating the prominence of CD133 in HCC.

Despite our growing understanding of the importance of a CD133$^+$ liver CSC population, the functional paths by which these cells promote hepatocarcinogenesis remains limited.

Since the intrinsic molecular mechanisms by which CSCs sustain tumor growth is believed to be inter-related with its tumor microenvironment, our present study aims at investigating the mechanism by which CD133$^+$ liver CSCs mediate tumor formation, self-renewal, and interaction with its niche. Toward this goal, RNA sequencing (RNA-seq) profiling was carried out to compare the differential gene expressions between CD133$^+$ liver CSCs and CD133$^-$ differentiated counterparts. Many of the differentially expressed genes common to the two samples encoded for secretory proteins, which we know represent major means of communication between cancer cells and the microenvironment. From our profiling, the most significantly deregulated gene that encodes for a secretory protein is annexin A3 (*ANXA3*), a gene we now show to be critical in promoting CSC-like properties in CD133$^+$ liver-CSC-driven HCC through both an autocrine and paracrine manner. ANXA3 belongs to the annexin family of Ca^{2+}-dependent phospholipid-binding proteins (Raynal and Pollard, 1994). It has been shown to possess the ability to promote angiogenesis (Park et al., 2005) and rat liver regeneration (Harashima et al., 2008). Upregulation of ANXA3 expression is detected in various tumor types including prostate, ovarian, and lung cancers (Köllermann et al., 2008; Schostak et al., 2009; Liu et al., 2009; Yan et al., 2010). In ovarian cancer, serum ANXA3 levels were significantly upregulated in diseased patients compared with healthy individuals (Yin et al., 2012). Further, overexpression of ANXA3 was found to contribute to platinum resistance in ovarian cancer (Yan et al., 2010). In HCC, ANXA3 was also found to be overexpressed in 5-fluorouracil (5-FU)-resistant cell lines (Yin et al., 2012) and to play a role in promoting tumorigenesis and resistance to chemotherapy (Pan et al., 2013). Nevertheless, the role of endogenous and secretory ANXA3 in the context of CD133$^+$ liver CSCs or HCC and the mechanism by which ANXA3 regulates CSC-like features has not been explored. Here, we investigated the clinical significance, functional role, and therapeutic implications of ANXA3 in CD133$^+$ liver-CSC-driven HCC. We identified caveolin-1-dependent endocytosis to mediate internalization of secretory ANXA3 into HCC cells, thereby activating a dysregulated JNK pathway to promote CSC-like properties. We also developed a monoclonal antibody specific against ANXA3 (anti-ANXA3 mAb) and showed in vivo that the use of this antibody alone or in combination with cisplatin could efficiently lead to a reduced ability of HCC cells to initiate tumor growth and self-renewal, concomitant with a decrease in liver CSC proportions.

RESULTS

Transcriptome Sequencing Profiling Identifies *ANXA3* to Be Preferentially Expressed in the CD133$^+$ Liver CSC Subset

To detect differential gene expression profiles between CD133$^+$ liver CSCs and their CD133$^-$ differentiated counterparts, we applied RNA-seq to investigate the sorted subsets isolated from two HCC cells, Huh7 and PLC8024. 95.61% of the reads mapped to the reference human genome (GRCh37/hg19) (Table S1). Using a stringent fold-change cutoff of >2 and <0.5 and a p value $\leq$ 0.05, 38 genes were found to be commonly de-regulated (Table S2). Pathway enrichment analysis identified critically over-represented pathways related to cancer, focal adhesion, extracellular matrix (ECM)-receptor interaction, drug metabolism, and ATP-binding casette (ABC) transporters in the deregulated gene set (Figure S1A). The same gene set was also surveyed using GSEA where *MAPK* signaling was found to be exclusively enriched in the CD133$^+$ liver CSC subset while CD133$^-$ cells was enriched for genes associated with hepatocyte differentiation (Figure S1B). Of the commonly differentially expressed genes, a good proportion of them (13/38; 34.2%) encode for secretory proteins (Table S2, red). And of these 13, annexin A3 (*ANXA3*) was the most significantly upregulated in the CD133$^+$ subset (Figure S1C) and was thus chosen for studies. Subsequent validation by qPCR confirmed preferential overexpression of *ANXA3* in CD133$^+$ liver CSCs isolated from a larger cohort of HCC cell lines and clinical samples (n = 8, Figure 1A). Endogenous and secretory proteomic ANXA3 levels were also likewise found elevated in the CD133$^+$ liver CSC subset (Figures 1B and 1C). Dual-color immunofluorescence (IF) confirmed a high degree of ANXA3 and CD133 co-localization in Huh7 (Figure 1D) and PLC8024 (Figure S1D). Concordant with this finding, expressions of ANXA3 and CD133 were also positively correlated across a panel of HCC cell lines (Figure 1E; Figure S1E).

Endogenous and Secretory ANXA3 Overexpression Is Tightly Associated with HCC Pathogenesis

We investigated endogenous ANXA3 expression in 83 matched primary HCC and non-tumor liver tissues. Approximately 50.6% (42/83) of the HCC specimens had ANXA3 upregulated (>1.5-fold) compared to non-tumor specimens. ANXA3 overexpression in HCC was significantly associated with advanced tumor stages (p = 0.027; Figure 1F; Table S3). Interestingly, secretory ANXA3 was also found to be progressively elevated from non-HCC patients (healthy subjects, hepatitis B virus [HBV] carriers, and patients with liver cirrhosis) to patients with early- and advanced-stage HCC, with ANXA3 overexpression in

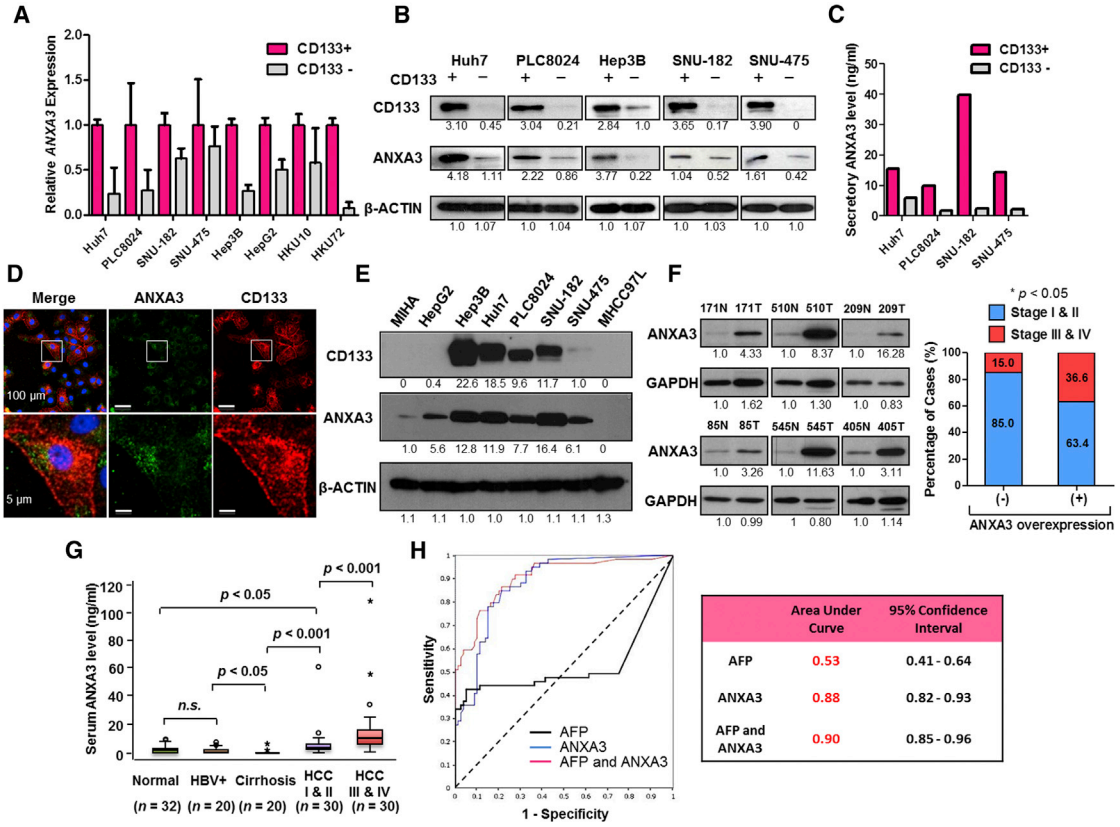

	Area Under Curve	95% Confidence Interval
AFP	0.53	0.41 - 0.64
ANXA3	0.88	0.82 - 0.93
AFP and ANXA3	0.90	0.85 - 0.96

Figure 1. Endogenous and Secretory Overexpression of ANXA3 Is Strongly Associated with HCC Pathogenesis

(A) Relative *ANXA3* expression in sorted CD133 subsets isolated from HCC cells and clinical samples by qPCR. Results represent mean ± SD of duplicate wells in three independent experiments.

(B) Western blot showing expression of ANXA3 in sorted CD133 subsets isolated from HCC cells.

(C) Secretory ANXA3 expression levels in sorted CD133 subsets isolated from HCC cells as detected by ELISA.

(D) Dual-color IF images of CD133 (red) and ANXA3 (green) in Huh7. Nuclei stained with DAPI (blue).

(E) Western blots showing expression of CD133 and ANXA3 in a panel of liver cancer cell lines.

(F) Western blot showing expression of ANXA3 in HCC (T) and matched non-tumor liver (N) specimens from six individual patients. Association between tumor stage and ANXA3 overexpression in HCC. *p < 0.05. Results represent mean ± SD from three independent experiments.

(G) Boxplots showing expression of ANXA3 in the sera collected from healthy individuals (normal), HBV carriers (HBV+), patients with liver cirrhosis, and patients with either early HCC (I & II) or advanced HCC (III & IV). Results represent mean ± SD of duplicate wells in three independent experiments.

(H) ROC curve analysis of the sensitivity and specificity of using AFP, ANXA3, or a combination of both for HCC diagnosis. Summary of ROC curve analysis with area under the curve (AUC) and 95% CI values.

See also Figure S1.

HCC sera tightly correlated with advanced tumor stages ($p < 0.001$), tumor sizes ($p = 0.005$), number of nodules ($p = 0.036$), and gender ($p = 0.011$) ($n = 132$). ANXA3 was found only at very low levels and was at times completely undetectable in sera collected from healthy individuals, HBV carriers, or patients with cirrhosis but without HCC (Figure 1G; Table S4). Alpha-fetoprotein (AFP) is the most widely used biomarker for HCC diagnosis. By receiver-operating characteristic (ROC) curve analysis, ANXA3 was found to be superior to AFP in distinguishing non-HCC from HCC (Figure 1H). The ROC curve analysis revealed that at the optimal cutoff value of 2.30 for ANXA3 alone, the sensitivity was 84.7% and the specificity was 78.8%, with an area under the curve (AUC) of 0.88 (95% confidence interval [CI], 0.82-0.93). The sensitivity was 42.3% and the specificity was 95.0% at the optimal cutoff value of 56.3 for AFP alone, with an AUC of 0.53 (95% CI, 0.41-0.64). The sensitivity was 93.2% and the specificity was 70% for the combination of ANXA3 and AFP, with an AUC of 0.90 (95% CI, 0.85-0.96).

Endogenous ANXA3 Regulates Both Cancer and Stem Cell-like Properties in HCC

To ascertain whether there is a causative relationship between ANXA3 overexpression and altered CSC-like phenotype in HCC, we generated stably overexpressed ANXA3 MIHA and MHCC97L cells and stably repressed ANXA3 Huh7 and PLC8024 cells (Figures S2A–S2C; sh-ANXA3 clones 244 and 246). ANXA3 knockdown in Huh7 and PLC8024 resulted in a significant decrease in the efficiency of the cells to form colonies, migrate, and invade. Conversely, stable ANXA3 overexpression resulted in opposing effects (Figures S2D–S2F). In addition, cells with ANXA3 suppressed displayed diminished abilities to induce hepatosphere formation in primary, secondary, and tertiary passages (Figure 2A; Figure S3A) and to potentiate resistance toward staurosporine (STS)-induced apoptosis, 5-FU, and cisplatin, chemotherapeutic agents commonly used in HCC therapy (Figures 2B and 2D; Figures S3B and S3D). Treatment of stably repressed ANXA3 cells with STS resulted in a marked reduction in cleaved caspase-3 and cleaved PARP (Figure 2C; Figure S3C). Treatment of Huh7 and PLC8024 cells with 5-FU and cisplatin resulted in an enriched ANXA3 subpopulation (Figure 2E; Figure S3E). Further, HCC cells with ANXA3 suppressed displayed an attenuated ability to mediate angiogenesis, as evidenced by capillary tube formation in endothelial cells (Figure 2F; Figure S3F). As a complementary model, similar assays were also performed in MIHA and MHCC97L cells with ANXA3 stably overexpressed, where enhanced abilities of the cells to confer cancer, stem cell-like, and metastatic traits were observed in the overexpressing clones (Figure 2; Figures S2 and S3).

ANXA3 Contributes to Augmented Tumorigenic and Metastatic Phenotype and Is Critical for Growth and Maintenance of the CD133$^+$ Liver CSC Subset

We then extended our studies in vivo, where HCC cells with ANXA3 manipulated were injected subcutaneously into nude mice to determine the role of ANXA3 in HCC tumor formation. Overexpression of ANXA3 in MHCC97L resulted in a profound increase in the ability of cells to initiate tumor growth, while knockdown of ANXA3 in Huh7 led to the complete inhibition of tumor growth (Figure 3A). Histological analysis revealed that the tumor xenografts displayed an HCC phenotype (Figure 3A), whereas immunohistochemistry (IHC) staining for ANXA3 confirmed preferential ANXA3 expression in the overexpressing clones (Figure 3B). MHCC97L-ANXA3 xenografts also displayed an enhanced proliferation rate, as confirmed by proliferating cell nuclear antigen (PCNA) staining (Figure 3B). Next, we examined the roles of ANXA3 in HCC metastasis in vivo by orthotopic implantation of the luciferase-labeled MHCC97L-EV- and MHCC97L-ANXA3-overexpressing cells into the livers of immunodeficient mice. Extrahepatic lung metastasis was monitored by ex vivo bioluminescence imaging. Lung metastasis was detected in six out of six mice in the ANXA3-overexpressing group, in contrast to only two out of six mice in the EV group (Figure 3C). Metastasis of tumor cells from the liver to lung was further confirmed by H&E staining with the presence of tumor nodules in the lungs (Figure 3C). Two cardinal properties of CSCs are tumor initiation and self-renewal, which can only be tested in vivo by limiting dilution and serial transplantation. To assess the degree by which enhanced ANXA3 supports growth and maintenance of CD133$^+$ liver CSCs, Huh7 cells with or without ANXA3 repressed were sorted into CD133$^+$ and CD133$^-$ subpopulations and injected subcutaneously into non-obese diabetic/severe combined immunodeficiency (NOD/SCID) mice at limited dilutions. CD133$^+$ANXA3^{low} cells exhibited attenuated tumor initiation at limiting dilutions when compared with CD133$^+$ANXA3^{high} cells, as evidenced by reduced tumor incidence, delayed tumor latency, and a lower estimated tumor-initiating cell frequency (Figure 3D). The reduced tumor-initiating ability of CD133$^+$ANXA3^{low} cells was comparable to that exhibited by CD133$^-$ANXA3^{high} cells, indicating the critical role of ANXA3 in mediating tumor initiation in vivo. Self-renewal ability of cells was then examined by serial transplantation of primary xenografts into secondary mouse recipients. Single cells isolated from the four groups were resorted into CD133$^+$ and CD133$^-$ subsets and injected subcutaneously into NOD/SCID mice at limited dilutions for secondary transplantation. CD133$^+$ANXA3^{low} cells had a diminished ability to reconstitute tumor formation in secondary transplantations compared with CD133$^+$ANXA3^{high} cells. Note that the estimated tumor-initiating cell number was only found enriched in secondary tumors generated from CD133$^+$ANXA3^{high} cells, but not in the other groups. After serial propagation, only one out of four mice in the CD133$^-$ANXA3^{high} group and none of the cells in the CD133$^-$ANXA3^{low} group were able to form secondary tumors, indicating that CD133$^+$ liver CSCs mediate self-renewal through ANXA3 (Figure 3D). This demonstrates that ANXA3 plays a critical role in driving tumor initiation, self-renewal, and metastasis in HCC.

Secretory ANXA3 Confers Tumorigenic, Metastatic, and Self-Renewal Abilities in HCC

Given that we found secretory ANXA3 to be detected in HCC clinical sera samples, we further sought to examine the functions of secretory ANXA3 in the maintenance of CSC-like properties in HCC. Conditioned medium from ANXA3-overexpressing MIHA or MHCC97L cells were harvested for co-culture with both CD133 and ANXA3 absent parental HCC cells (Figure 4A). In addition, to provide

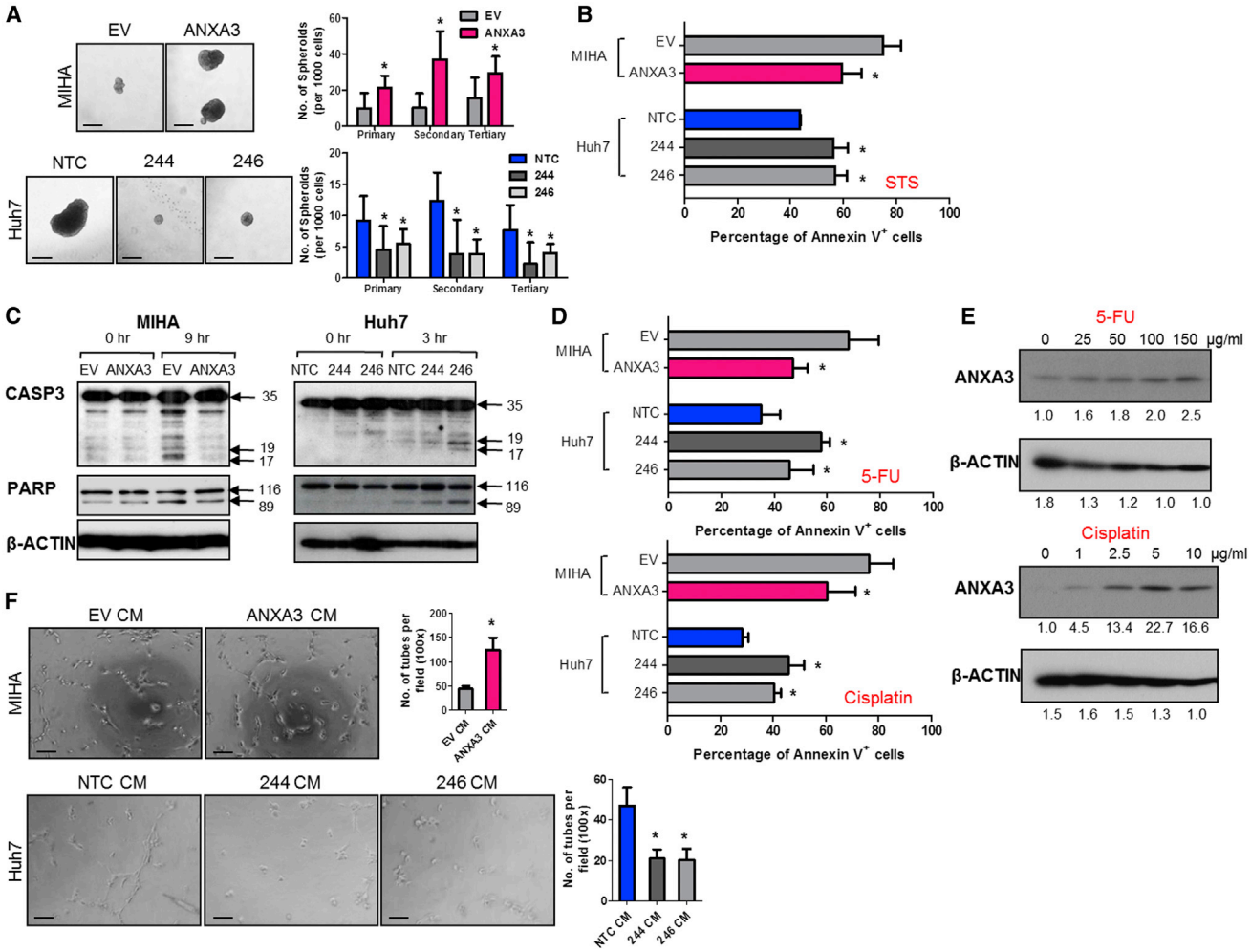

Figure 2. Endogenous ANXA3 Confers Enhanced Cancer and Stem Cell-like Properties in HCC

(A) Quantification of hepatospheres in HCC cells with ANXA3 stably expressed (MIHA EV and ANXA3 O/E) or repressed (Huh7 NTC and ANXA3 knockdown clones 244 and 246). *$p < 0.05$. EV, empty vector; O/E, overexpression; NTC, non-target control. Scale bar, 100 μm. Results represent mean ± SD of 12 replicates in three independent experiments.

(B) Percentage of Annexin-V-positive cells in MIHA and Huh7 with ANXA3 stably expressed and repressed, respectively, following STS treatment. Results represent mean ± SD of three independent experiments.

(C) Western blot showing expression of total and cleaved caspase-3 and PARP after STS treatment.

(D) Percentage of Annexin-V-positive cells in MIHA and Huh7 with ANXA3 stably expressed and repressed, respectively, following 5-FU and cisplatin treatment. Results represent mean ± SD of three independent experiments.

(E) Western blot showing expression of ANXA3 in Huh7 following treatment with increasing concentrations of 5-FU and cisplatin.

(F) Quantification of capillary tubes formed by human umbilical vein endothelial cells (HUVECs) following treatment with supernatant collected from MIHA and Huh7 with ANXA3 stably expressed and repressed, respectively. *$p < 0.05$. Scale bar, 100 μm. Results represent mean ± SD of duplicate wells in three independent experiments.

See also Figures S2 and S3.

direct evidence that it is indeed secretory ANXA3, and not other factors in the conditioned medium, that is responsible for promoting these properties, ANXA3-absent HCC cells were also treated with recombinant ANXA3 proteins (Figure 4A). HCC cells co-cultured with conditioned medium collected from ANXA3-overexpressing cells exhibited a greater ability to migrate, invade (Figure 4B), form hepatospheres (Figure 4C), and resist apoptosis as well as chemotherapy (Figure 4D), as compared to HCC cells co-cultured with conditioned medium collected from controls. Similar results were obtained when MIHA cells, absent of both ANXA3 and CD133, showed enhanced ability

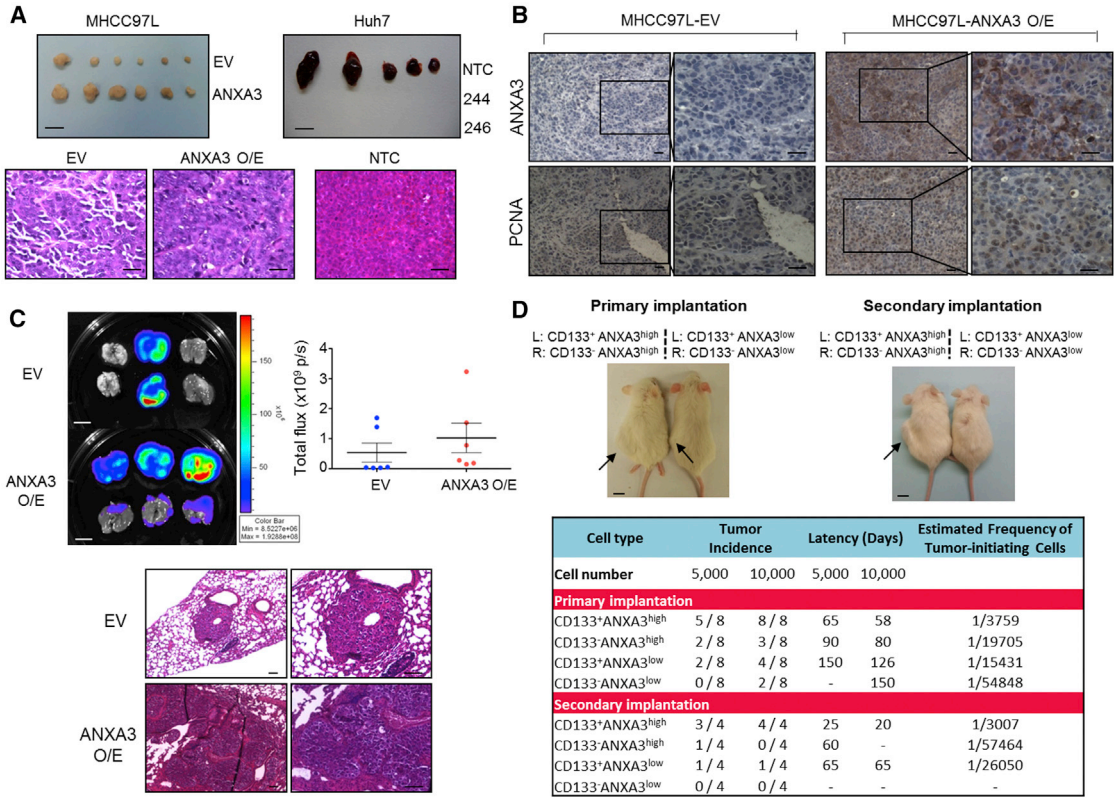

Cell type	Tumor Incidence		Latency (Days)		Estimated Frequency of Tumor-initiating Cells
Cell number	5,000	10,000	5,000	10,000	
Primary implantation					
CD133$^+$ANXA3^{high}	5 / 8	8 / 8	65	58	1/3759
CD133$^-$ANXA3^{high}	2 / 8	3 / 8	90	80	1/19705
CD133$^+$ANXA3^{low}	2 / 8	4 / 8	150	126	1/15431
CD133$^-$ANXA3^{low}	0 / 8	2 / 8	-	150	1/54848
Secondary implantation					
CD133$^+$ANXA3^{high}	3 / 4	4 / 4	25	20	1/3007
CD133$^-$ANXA3^{high}	1 / 4	0 / 4	60	-	1/57464
CD133$^+$ANXA3^{low}	1 / 4	1 / 4	65	65	1/26050
CD133$^-$ANXA3^{low}	0 / 4	0 / 4	-	-	-

Figure 3. Endogenous ANXA3 Contributes to Augmented Tumor-Initiating, Self-Renewal, and Metastatic Potential In Vivo

(A) Top: representative xenograft tumors derived from MHCC97L-EV and -ANXA3 O/E or Huh7-NTC and -ANXA3 knockdown clones 244 and 246 cells 4 weeks after subcutaneous injection (n = 5–6). Scale bar, 1 cm. Bottom: H&E- images of tumors derived from MHCC97L-EV, -ANXA3 O/E, and Huh7-NTC cells. Scale bar, 200 μm.

(B) IHC staining for expression of ANXA3 and PCNA in the resected xenograft tumors derived from MHCC97L-EV and -ANXA3 O/E cells. Scale bar, 200 μm.

(C) Ex vivo imaging of lungs harvested from mice that received orthotopic injections of MHCC97L-EV or -ANXA3 O/E cells in the liver. Luciferase signals shown as dot plot. H&E images of lung tissue harvested. Scale bars represent 1 cm (top) and 100 μm (bottom). Results represent mean ± SD of six mice from one independent experiment.

(D) Top: images of tumors (black arrows) formed in NOD/SCID mice injected subcutaneously with CD133$^+$ANXA3$^+$, CD133$^+$ANXA3$^-$, CD133$^-$ANXA3$^+$, and CD133$^-$ANXA3$^-$ cells isolated from Huh7 (picture representative of a 5,000-cell injection) (n = 8 for primary and n = 4 for secondary implantations). Scale bar, 1 cm. Bottom: engraftment rates of CD133$^+$ and CD133$^-$ subsets with or without ANXA3 repressed in Huh7. See also Figures S2 and S3.

to migrate, form hepatospheres, and induce capillary tube formation following treatment with recombinant ANXA3 proteins (Figure 4E). Our in vitro observations were also substantiated in vivo. MHCC97L cells resuspended in either conditioned medium collected from ANXA3-overexpressing or EV controls were injected subcutaneously into immunodeficient mice. For 2 weeks following inoculation of cells, concentrated conditioned media were injected subcutaneously at the site of the tumor inoculation. Tumor-initiating ability was significantly potentiated in MHCC97L cells co-cultured with ANXA3-containing conditioned medium, where tumors were detected in all eight animals. In contrast, only four out of eight mice inoculated with MHCC97L cells mixed with EV-control conditioned medium developed tumor nodules. ANXA3-containing conditioned medium not only enhanced the tumor-initiating capacity of these cells but also promoted tumor growth, as evidenced by the larger tumors that were formed (Figure 4F). Collectively, this suggests that secretory ANXA3 is indeed pivotal for tumor initiation, growth, metastasis, and chemoresistance.

Exogenous ANXA3 Is Internalized through Caveolin-1-Dependent Endocytosis

Next, we delineated the mechanism by which exogenous ANXA3 binds to and enters cells to exert its oncogenic

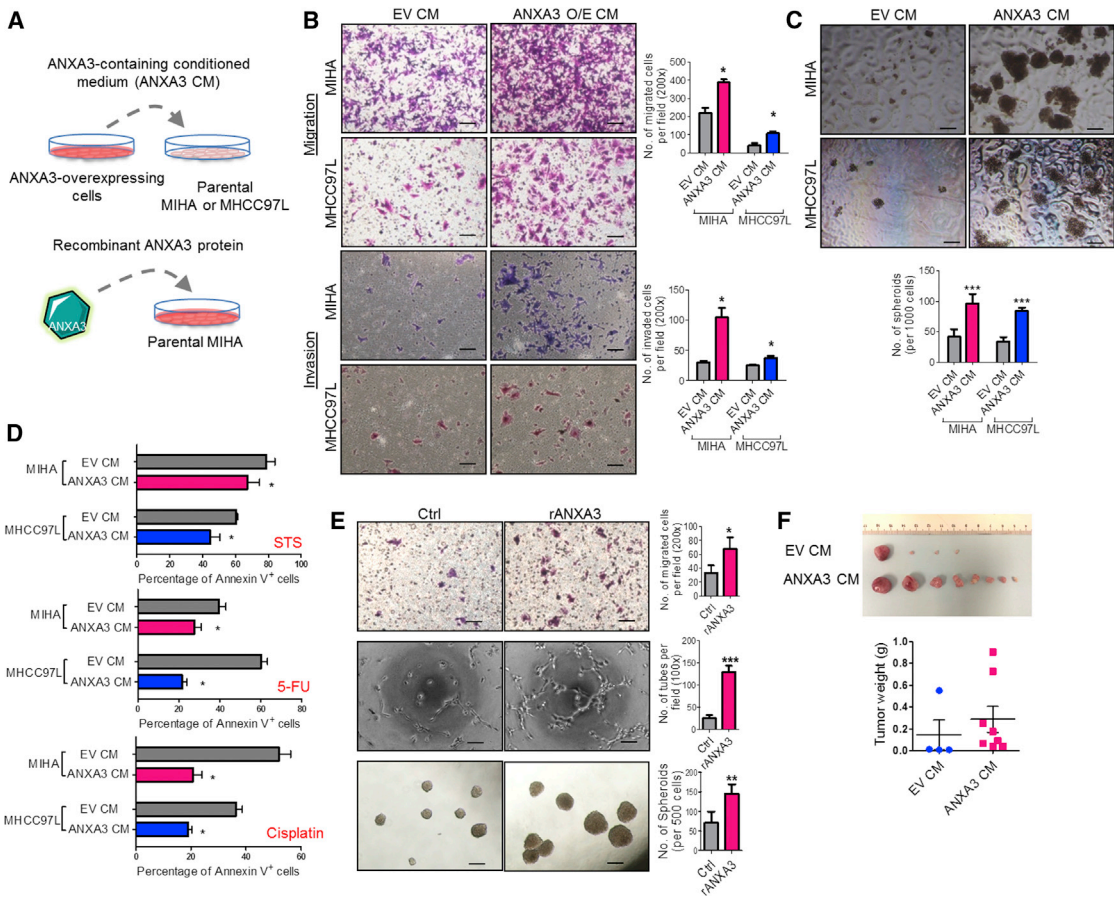

Figure 4. Secretory ANXA3 Confers Enhanced Cancer and Stem Cell-like Properties in HCC In Vitro and In Vivo

(A) Secretory ANXA3 overexpression and recombinant ANXA3 model systems.

(B) Quantification of number of MIHA and MHCC97L cells that migrated or invaded following co-culture with empty vector control medium (EV CM) or ANXA3-containing conditioned medium (ANXA3 O/E CM). *$p < 0.05$. Scale bar, 200 μm. Results represent mean ± SD from three independent experiments.

(C) Quantification of hepatospheres formed following co-culture with EV CM or ANXA3 O/E CM. ***$p < 0.001$. Scale bar, 100 μm. Results represent mean ± SD of 12 replicates in three independent experiments.

(D) Percentage of Annexin-V-positive cells in MIHA and MHCC97L co-cultured with EV CM or ANXA3 O/E CM, following treatment with STS, 5-FU, or cisplatin. Results represent mean ± SD of three independent experiments.

(E) Top and bottom: quantification of number of MIHA that migrated and formed hepatospheres following treatment with recombinant ANXA3 protein (rANXA3). *$p < 0.05$ and **$p < 0.01$. Results represent mean ± SD from three independent experiments. Middle: quantification of capillary tubes formed by HUVECs following treatment with rANXA3. ***$p < 0.001$. Scale bars represent 200 μm (top) and 100 μm (middle and bottom). Results represent mean ± SD of duplicate wells in three independent experiments.

(F) Representative xenograft tumors derived from MHCC97L cells co-cultured with EV CM or ANXA3 O/E CM 4 weeks after subcutaneous injection (n = 8). Dot plot shows the tumor weight of each xenograft. Results represent mean ± SD of eight mice from one independent experiment.

effects to promote HCC. We first confirmed that exogenous ANXA3 was indeed internalized. Recombinant SNAP-tagged ANXA3 protein was first labeled with fluorophore (red). PLC8024 HCC cells were also labeled with Vybrant carboxyfluorescein diacetate (CFDA) succinimidyl ester cell tracer dye (green). Following co-culture of fluorophore-tagged recombinant ANXA3 protein with fluorescein-isothiocyanate-labeled PLC8024 cells, SNAP-tagged ANXA3 proteins were clearly detected on both the membrane and in the cytoplasm of PLC8024 cells by confocal microscopy (Figure 5A). This observation was further substantiated by western blot where subcellular fractionation of HCC cells co-cultured with recombinant ANXA3 protein was analyzed. FLAG-tagged ANXA3 proteins present in the two fractions were pulled down by immunoprecipitation with FLAG-conjugated antibodies and subjected to

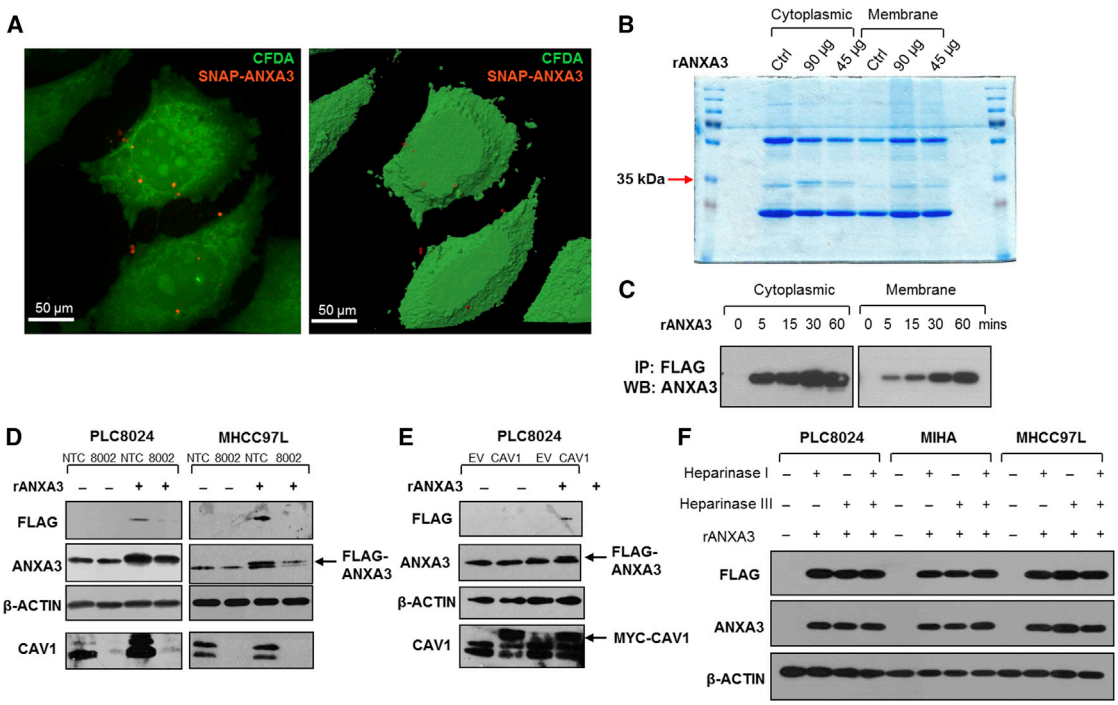

Figure 5. Exogenous ANXA3 Is Internalized through Caveolin-1-Dependent Endocytosis

(A) Representative 2D and 3D confocal microscopy images of CFDA-stained PLC8024 following co-culture with SNAP-tagged ANXA3 proteins (SNAP-ANXA3).

(B) Coomassie-blue-stained SDS-PAGE gel showing cytoplasmic and membrane sub-fractions of PLC8024 treated with 45 or 90 μg of recombinant FLAG-ANXA3 protein (rANXA3). Arrow depicts 35-kDa band, which corresponds to rANXA3.

(C) Western blot showing expression of ANXA3 in cytoplasmic and membrane sub-factions of PLC8024 treated with 90 μg of rANXA3 and immunoprecipitated by FLAG antibody.

(D) Western blot showing expression of FLAG, ANXA3, and CAV1 in PLC8024 and MHCC97L with or without CAV1 stably repressed and with or without rANXA3 treatment.

(E) Western blot showing expression of FLAG, ANXA3, and CAV1 in PLC8024 with or without Myc-CAV1 stably overexpressed and with or without rANXA3 treatment.

(F) Western blot showing expression of FLAG and ANXA3 in PLC8024, MIHA, and MHCC97L co-treated with rANXA3, heparinase I, heparinase II, or their combination.

Representative images from three independent experiments are shown for all experiments.

SDS-PAGE. A 35-kDa band, concordant with the size of ANXA3 protein, was identified solely in the cytoplasm in the Coomassie-blue-stained gel, but not in the untreated control. Intensity of this band increased in a dose-dependent manner when increasingly more ANXA3 protein was added (Figure 5B). The identity of the band was confirmed to be ANXA3 by western blot and mass spectrometry analysis (data not shown). Recombinant ANXA3 was detected in both cytoplasmic and membrane subfractions, suggesting accumulating levels of the protein inside the cell over time (Figure 5C).

Endocytosis represents a major mechanism for internalization of extracellular cargoes. Caveolin-1 proteins are main components of caveolae that can facilitate internalization of glycosylphosphatidylinositol (GPI)-anchor proteins and receptors into target cells through caveolar endocytosis. In view of the ability of ANXA3 protein to bind phospholipid membrane, we hypothesized that exogenous ANXA3 proteins are recruited to the caveolae and internalized through this mechanism. To this goal, caveolin-1 (CAV1) was stably repressed by small hairpin RNA knockdown. PLC8024 and MHCC97L cells with CAV1 depleted and co-cultured with recombinant FLAG-tagged ANXA3 protein had a reduced ability to bind and internalize exogenous ANXA3 as compared to HCC cells transfected with non-target controls, as indicated by decreased FLAG and ANXA3 expression levels (Figure 5D; sh-CAV1 clones 8001 and 8002). In contrast, overexpression of CAV1 in PLC8024 cells resulted in an increased internalization of FLAG-tagged ANA3 proteins (Figure 5E). Since previous reports have revealed other members of the annexin family (ANXA1, A2, A4, A5, and A6) to commonly bind to

glycosaminoglycans (GAGs) such as heparin sulfate chains, we also explored whether ANXA3 could also be internalized via heparin sulfate proteoglycan (HSPG)-mediated endocytosis. PLC8024, MIHA, and MHCC97L cells treated with heparinase I, heparinase III, or their combination and co-cultured with recombinant FLAG-tagged ANXA3 protein did not alter the amount of ANXA3 proteins internalized (Figure 5F), suggesting that entry of exogenous of ANXA3 in HCC is dependent on caveolin-1-mediated, but not HSPG-mediated, endocytosis.

ANXA3 Induces a Feed-Forward Loop that Is Mediated by the MKK4/JNK Signaling Cascade

In an effort to characterize the molecular mechanism by which ANXA3 drives CSC-like properties in HCC, mRNA expression profiling was performed to compare the gene expression profiles of PLC8024 cells with or without ANXA3 repressed (Figure S4A; NTC versus sh-ANXA3 clone 246). Using a fold-change cutoff of >3, 2,372 differentially expressed genes were identified. Subsequent pathway analysis found many of the deregulated genes to be closely associated with *JNK/AP-1* and *MAPK*, pathways, which have previously been shown to play a critical role in HCC pathogenesis (Figure 6A; Figure S4B) (Hagiwara et al., 2012; Jin et al., 2013). Deregulation of key players of the JNK pathway, including p-MKK4, JNK kinase activity, c-MYC, and p21, was subsequently validated by western blot in HCC cells with ANXA3 repressed (Huh7 and PLC8024) or overexpressed (MIHA) (Figure 6B). Similar to results obtained from ANXA3-overexpressing cells, the addition of exogenous ANXA3 proteins in CD133- and ANXA3-absent MIHA cells or culturing of the cells with conditioned medium collected from ANXA3-overexpressing cells resulted in JNK pathway activation, as evidenced by an increase in JNK activity, increased c-MYC expression, and reduced p21 expression (Figure 6C). A luciferase-reporter construct consisting of a consensus sequence of AP-1 binding site was transfected into Huh7 cells with or without ANXA3 repressed. Activity of AP-1, a known downstream target of JNK, was significantly reduced in the ANXA3-knockdown clones, further suggestive of the critical role of the ANXA3-JNK axis in $CD133^+$ liver-CSC-driven HCC (Figure 6D). Consistent with this, we also found p-JNK to be preferentially expressed in $CD133^+$ HCC cells (Figure S4C), while dual-color IF confirmed co-localization of ANXA3 and p-JNK, as well as CD133 and p-JNK in both Huh7 and PLC8024 cells (Figure 6E; Figures S4D and S4E). To substantiate the importance of the JNK/AP-1 pathway in ANXA3-driven HCC, we performed rescue experiments using the JNK-specific inhibitor (JNKi) SP600125. JNKi suppressed the oncogenic properties conferred by ANXA3 overexpression, as evidenced by the diminished abilities of HCC cells to form colonies, migrate, invade, induce angiogenesis, form hepatospheres, and resist apoptosis and chemotherapy (Figures 6F–6J). Interestingly, treatment of parental HCC cells or HCC cells overexpressing ANXA3 with JNKi resulted in not only a reduction in JNK activity and modulation of downstream target genes (c-MYC and p21) but also a marked decrease in ANXA3 expression, suggesting that ANXA3 induces a feed-forward loop that is mediated by MKK4/JNK signaling (Figures 6K–6L).

ANXA3 Neutralization Suppresses Growth and Self-Renewal of HCC In Vivo, Sensitizes HCC to Chemotherapy, and Eradicates the CD133 Liver CSC Subset

In light of the implications of ANXA3 in $CD133^+$ liver CSCs and in HCC, we subsequently developed a monoclonal antibody specific against ANXA3 (anti-ANXA3 mAb) and tested for its application as a therapeutic treatment against HCC. Specificity of the antibody was confirmed by western blot on a panel of HCC cell lines where a single 33-kDa band was detected, corresponding to ANXA3 (Figure 7A). The expression levels of ANXA3 obtained were concordant with findings using a commercially validated ANXA3 antibody. Cell proliferation rates of CD133- and ANXA3-positive Huh7 cells were significantly inhibited with the addition of anti-ANXA3 mAb, while the CD133- and ANXA3-absent immortalized normal liver cell line MIHA remained unresponsive (Figure 7B). Treatment of Huh7 with anti-ANXA3 mAb resulted in a marked increase in apoptotic cells, suggesting that cell death was a factor causing the inhibition of cell proliferation (Figure 7C). In addition, anti-ANXA3 mAb also reduced the abilities of HCC cells to migrate, invade, induce angiogenesis, and form hepatospheres (Figures 7D–7F). HCC cells treated with a combination of anti-ANXA3 mAb and cisplatin synergistically inhibited cell proliferation in vitro and sensitized HCC cells to cisplatin (Figure 7G). Consistently, a similar trend was also observed when anti-ANXA3 mAb was used for treatment of secretory ANXA3. MIHA and MHCC97L cells, both negative for CD133 and ANXA3, were stably transfected with ANXA3 or EV control. Conditioned medium from these cells were then collected and used for various functional experiments. Addition of ANXA3 mAb in HCC cells treated with conditioned medium collected from ANXA3-overexpressing cells resulted in a reduced ability of the cells to migrate, invade, induce angiogenesis, form hepatospheres, and resist apoptosis and chemotherapy (Figures S5A and S5B). This observation was confirmed in vivo when treatment of Huh7 xenografts in immunodeficient mice with anti-ANXA3 mAb alone or in combination with cisplatin resulted in a marked reduction in tumor volume (Figure 7H; Figure S5C).

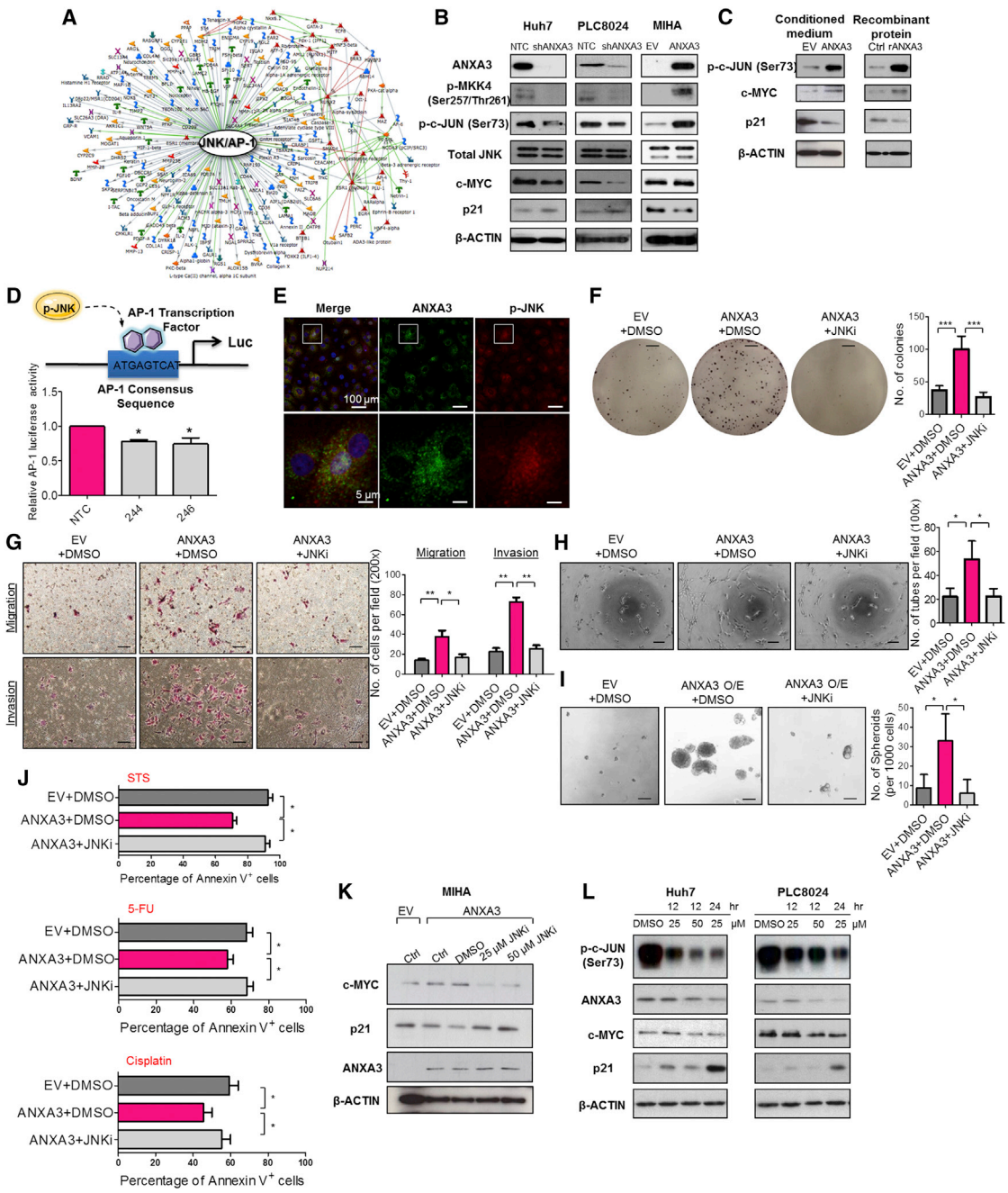

Figure 6. Increased ANXA3 Expression Enhances JNK Signaling in CD133$^+$ Liver CSCs

(A) Gene expression profiling coupled with GeneGo Metacore analysis in PLC8024 with or without ANXA3 repressed identified a deregulated *JNK/AP-1* signaling network.

(B) Western blot showing expression of ANXA3, a key player in the JNK pathway (p-MKK4, JNK kinase activity, total JNK), and its downstream targets (c-MYC and p21) in Huh7, PLC8024, and MIHA with or without ANXA3 stably repressed or overexpressed.

(C) JNK kinase assay and western blot analysis of activity and expression of JNK-related proteins in MIHA co-cultured with ANXA3 O/E CM, rANXA3, or their controls.

(D) Luciferase reporter assay for activity of AP-1 transcription factor in Huh7 with or without ANXA3 stably repressed. *$p < 0.05$. Results represent mean ± SD from triplicate wells in three independent experiments.

(E) Dual-color IF images of ANXA3 (green) and p-JNK (red) in Huh7. Nuclei stained with DAPI (blue).

(legend continued on next page)

Tumor growth was markedly suppressed in mice treated with increasing concentrations of anti-ANXA3 mAb. When anti-ANXA3 mAb was administered in combination with cisplatin, the growth of the tumor engraftments was inhibited by as much as 90% compared with the controls (PBS or immunoglobulin G [IgG]). Although cisplatin treatment alone led to a bigger reduction in tumor volume as compared to anti-ANXA3 mAb (Figure 7H), the residual xenografts, when serially transplanted into secondary mouse recipients, formed the largest tumors (Figure 7I). Residual xenografts from anti-ANXA3 mAb or mAb and cisplatin treatment failed to give rise to tumors in serial transplantations (Figure 7I), suggesting that a subset of CSCs is enriched by chemotherapy treatment. Subsequent analysis of the residual xenografts by flow cytometry for CD133 confirmed this hypothesis, where proportion of $CD133^+$ cells was found enriched after chemotherapy, while the proportion of $CD133^+$ cells decreased following treatment with anti-ANXA3 mAb alone or in combination with cisplatin (Figure 7J; Figure S5E). In addition to CD133, other liver CSC markers known to have overlapping expression with CD133, including CD24 (Lee et al., 2011) and EpCAM (Yamashita et al., 2009), were also found to be diminished upon antibody treatment (Figure S5F). H&E staining and IHC were performed on tissue sections from the resected tumor residuals (Figure 7K; Figure S5D). Necrosis was only observed in the xenografts treated with anti-ANXA3 mAb alone or in combination with cisplatin. ANXA3 expression was increased in cisplatin-treated xenografts but was markedly reduced in anti-ANXA3 mAb-treated mice. A concomitant decrease in PCNA was also observed in xenografts treated with anti-ANXA3 mAb with or without cisplatin, indicative of attenuated proliferative potential. None of the mice showed signs of disability, behavior abnormalities, or significant changes in body weight. Compared to untreated control or IgG-treated mice, no additional tissue damage was observed in other vital organs (Figure S5G). Mechanistically, treatment of HCC cells with anti-ANXA3 mAb in vitro and in vivo similarly led to a suppressed JNK pathway (Figure 7L).

DISCUSSION

Frequent tumor relapse in multiple tumor types has now been attributed to the presence of residual CSCs after conventional treatments. We and others have previously identified CD133 to mark a liver CSC subpopulation in HCC (Ma et al., 2007, 2010). Yet, the functional paths by which these cells promote hepatocarcinogenesis remain limited, significantly impeding our efforts in developing CSC-specific therapies. We characterized the mRNA transcriptome of $CD133^+$ and $CD133^-$ subpopulations in HCC by RNA-seq. Pathway enrichment analysis found the $CD133^+$ subset to be tightly associated with an activated *MAPK* pathway, which is in concordant with our previous study, where we found CD133 to promote angiogenesis through IL-8-activated ERK (Tang et al., 2012). In addition, our $CD133^-$ non-CSC subset was also found to be enriched for genes critical in hepatocyte differentiation. This result is also consistent with our finding where $CD133^-$ cells were found to be unable to differentiate into skeletal and cardiac lineages, while in contrast, $CD133^+$ liver CSCs could efficiently differentiate into non-hepatocyte-like, angiomyogenic-like cells following cell-directed differentiation in vitro (Ma et al., 2007), suggesting that $CD133^-$ cells exist in a terminally differentiated state. Of interest, one-third of the differentially expressed genes identified were found to encode for secretory proteins. There is accumulating data to show that maintenance of cancer and stemness properties is dependent on the microenvironment in which deregulated secreting factors can communicate through paracrine or autocrine signaling. Given the importance of secretory factors in modulating CSC features and that they can be found accessible in the conditioned media of cells or serum in patients, thus making them prime

(F) Quantification of number of colonies formed in the indicated stable cell lines with or without JNK inhibitor. ***$p < 0.001$. Scale bar, 5 mm. Results represent mean ± SD from triplicate wells in three independent experiments.
(G) Quantification of number of cells that migrated or invaded following co-culture with or without JNK inhibitor. *$p < 0.05$ and *$p < 0.01$. Scale bar, 100 μm. Results represent mean ± SD from three independent experiments.
(H) Quantification of capillary tubes formed by HUVECs following treatment with supernatant collected from the indicated cell lines with or without JNK inhibitor. *$p < 0.05$. Scale bar, 100 μm. Results represent mean ± SD of duplicate wells in three independent experiments.
(I) Quantification of hepatospheres with or without JNK inhibitor. Scale bar, 100 μm. Results represent mean ± SD of 12 replicates in three independent experiments.
(J) Percentage of Annexin-V-positive cells in the indicated stable cell lines with or without JNK inhibitor, following treatment with STS, 5-FU, or cisplatin. Results represent mean ± SD of three independent experiments.
(K and L) Western blot showing expression of ANXA3, c-MYC, and p21 in ANXA3-overexpressing MIHA (K) and parental Huh7 and PLC8024 (L) treated with 25 or 50 μM JNK inhibitor (SP600125).
See also Figure S4.

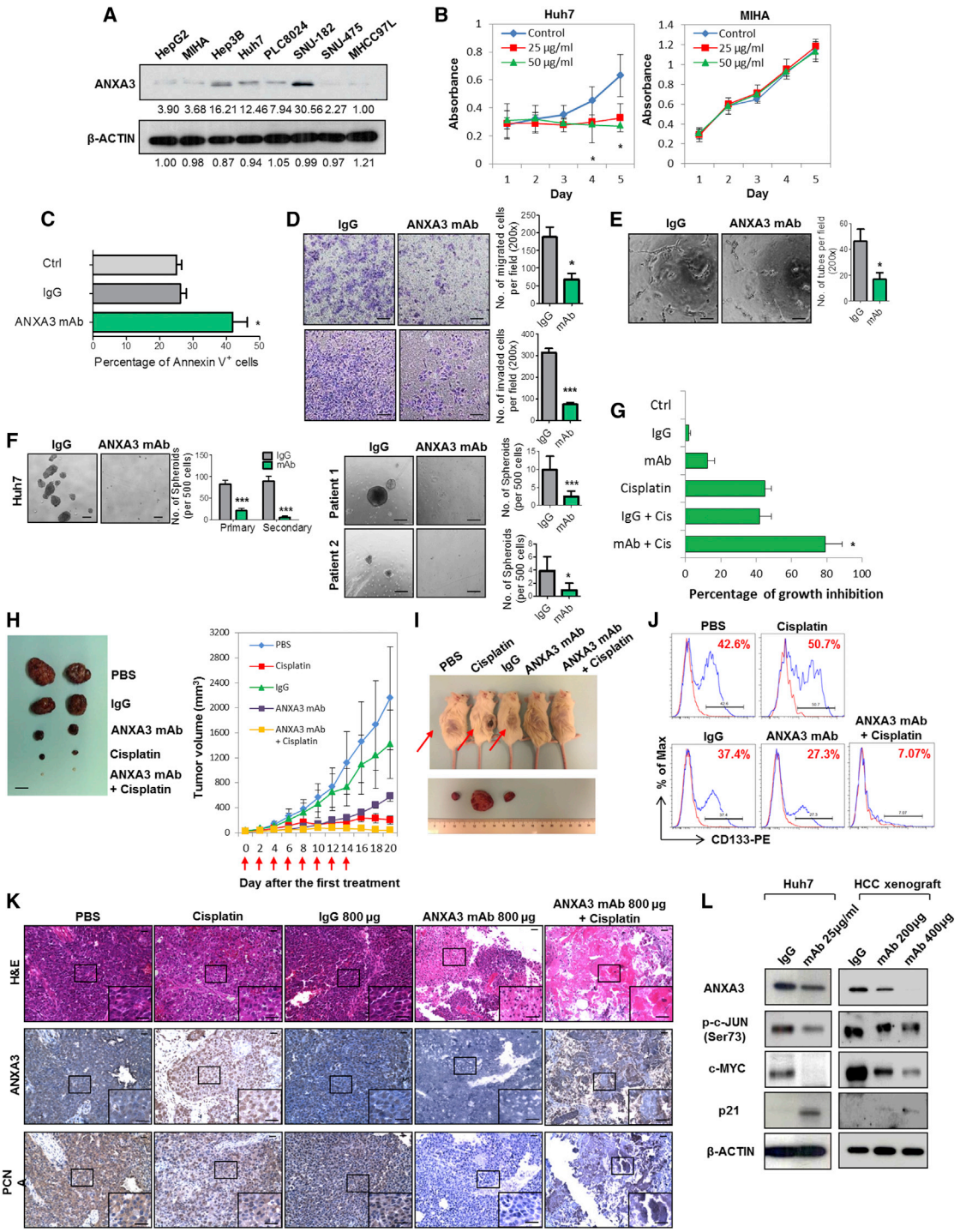

Figure 7. ANXA3 Ablation Reduces Cancer and Stem Cell-like Properties in HCC In Vitro, Attenuates Tumor Formation In Vivo, and Decreases Liver CSC Subpopulations

(A) Western blot showing specificity of the ANXA3 monoclonal antibody in a panel of liver cell lines.

(B) XTT assay showing growth rates of Huh7 and MIHA in the absence or presence of ANXA3 mAb. *$p < 0.05$. Results represent mean ± SD of triplicate wells in three independent experiments.

(C) Percentage of Annexin-V-positive cells in Huh7 following treatment with 25 μg/ml IgG control or ANXA3 mAb. Results represent mean ± SD from three independent experiments.

(legend continued on next page)

druggable targets for novel therapy development, we focused our studies in this area.

The focus of ANXA3 research in the past has centered on its expression in various diseases. A number of studies have found ANXA3 to be frequently overexpressed in ovarian, breast, colon, lung, gastric, gallbladder, testicular, and urothelial cancers (Köllermann et al., 2008; Schostak et al., 2009; Liu et al., 2009; Yan et al., 2010; Wu et al., 2013). In contrast, ANXA3 was also found to be downregulated in prostate and papillary thyroid cancers (Wu et al., 2013). In recent years, a small number of studies have identified ANXA3 to be secreted, where low levels of ANXA3 present in the urine were found to have diagnostic significance for early prostate cancer (Schostak et al., 2009; Yin et al., 2012) and secretion of ANXA3 from ovarian cancer cells is associated with platinum resistance. Here, we found ANXA3 to represent the most significantly upregulated gene that encoded for a secretory protein in the $CD133^+$ liver CSC subset. Haraguchi et al. also likewise found ANXA3 to be preferentially expressed in the side population (SP) isolated from Huh7 cells (Haraguchi et al., 2006). SP cells from HCC were subsequently characterized to also express CD133. Specifically in HCC, Tong et al. found ANXA3 to be upregulated in 5-FU-resistant HCC cells and that silencing of ANXA3 by RNAi resulted in enhanced sensitivity of HCC cells to chemotherapy (Tong et al., 2012). By mass-spectrometry-based profiling, Tsai et al. identified several altered proteins, including ANXA3, to be highly expressed in Huh7 $CD133^+$ liver CSCs (Tsai et al., 2012). Pan et al. also reported the preferential upregulation of endogenous ANXA3 in $CD133^+$ cells isolated from Huh7 and that ANXA3 is required for sphere formation, tumor initiation, migration, invasion, and chemoresistance in HCC cells via a deregulated HIF1α/NOTCH pathway (Pan et al., 2013, 2015). These studies do suggest the importance of ANXA3 in $CD133^+$ liver CSCs and in HCC. However, since the authors did not perform in vivo transplantation and serial propagations at limited dilutions, which remains the gold standard to test tumorigenicity and self-renewal, the reports are at best suggestive. Further, their work only looked at cytoplasmic ANXA3. Our present study definitively reports the functional role of ANXA3 in mediating CSC-like properties in HCC. Our work also demonstrates the clinical relevance and functional significance of secretory ANXA3 in HCC. Whether ANXA3 can be developed as a standalone biomarker or used in combination with AFP for clinical use warrants further investigation in a larger patient sample cohort. Our functional studies identified the role of endogenous and exogenous ANXA3 in conferring CSC-like properties.

Next, we unraveled a mechanism by which exogenous ANXA3 proteins are internalized in HCC cells and characterized the mechanism by which ANXA3 promotes CSC-like properties following its internalization. There has been no study regarding the route of entry of exogenous ANXA3 in any cell type thus far. We found exogenous ANXA3 to be internalized into HCC cells through caveolin-1-mediated, but not HSPG-mediated, endocytosis. Consistently, data obtained from our previous mRNA expression profiles (Tang et al., 2012) also found caveolin-1 to be upregulated in the $CD133^+$ subsets, suggesting an autocrine regulation through the secretion and internalization of ANXA3. Through gene expression profiling coupled with functional rescue experiments, we found ANXA3 to activate the JNK pathway in $CD133^+$ liver CSCs. Multiple studies have found JNK to drive HCC (Hagiwara et al., 2012; Jin et al., 2013). One recent study also found JNK activation to regulate self-renewal and tumor

(D) Quantification of cells that migrated or invaded following treatment with IgG control or ANXA3 mAb. $^*p < 0.05$ and $^{***}p < 0.001$. Scale bar, 100 μm. Results represent mean ± SD from three independent experiments.
(E) Quantification of capillary tubes formed by HUVECs following treatment with supernatant collected from HCC cells treated with IgG control or ANXA3 mAb. $^*p < 0.05$. Scale bar, 100 μm. Results represent mean ± SD of duplicate wells in three independent experiments.
(F) Quantification of hepatospheres in Huh7 and clinical samples following treatment with IgG control or ANXA3 mAb. $^*p < 0.05$ and $^{***}p < 0.01$. Scale bar, 100 μm. Results represent mean ± SD of 12 replicates in three independent experiments.
(G) XTT assay showing percentage growth inhibition in Huh7 following treatment with ANXA3 mAb, cisplatin, their combination, or their controls. $^*p < 0.05$. Results represent mean ± SD of triplicate wells in three independent experiments.
(H) Representative xenograft tumors resected from mice treated with PBS, IgG control, ANXA3 mAb, cisplatin, or a combination of ANXA3 mAb and cisplatin (n = 5). Graph of average tumor volumes of mice along treatment course. Red arrows indicate the days when treatment was administered. Scale bar, 1 cm. Results represent mean ± SD of five mice from one independent experiment.
(I) Representative images of secondary tumors (black arrows) formed in NOD/SCID mice injected subcutaneously with cells harvested from residual primary tumors shown in (A).
(J) Flow cytometry for CD133 in residual xenografts of the indicated treatment groups.
(K) H&E and IHC staining for expression of ANXA3 and PCNA in the resected xenograft tumors. Scale bar, 200 μm.
(L) JNK kinase assay and western blot analysis of activity and expression of JNK-related proteins in Huh7 or HCC xenografts resected from mice treated with IgG control or ANXA3 mAb. Images shown of data gathered from n = 5 mice for in vivo studies shown in (H)–(K).
See also Figure S5.

initiation in CD133$^+$ glioblastoma stem cells (Yoon et al., 2012). Through rescue experiments, we substantiated the importance of JNK pathway in mediating ANXA3-driven CSC-like features. Blockade of the JNK pathway in turn caused a reduction of ANXA3 expression, suggesting the existence of a positive feedback loop regulating ANXA3 expression in HCC. Our group has also initiated some studies to clarify the mechanism by which ANXA3 is secreted, and we have pilot data (not shown) to suggest that ANXA3 is secreted from CD133-expressing HCC cells as exosomes. However, more work is needed to validate this observation.

The last part of our study centered on the therapeutic potential of targeting secretory ANXA3 through the use of a neutralizing antibody. Here, we provide data to show that ANXA3 sequestration by our newly developed mAb resulted in attenuation of CSC-like properties via the suppression of JNK. Not only did the anti-ANA3 mAb suppress CSC properties, but also CSC content was depleted with a marked reduction in the expression of CD133, CD24, and EpCAM. We also found that when administered in combination with cisplatin, the mAb would exert a synergistic inhibitory effect against HCC. Emerging studies have suggested the possibility of CSC replenishment through dedifferentiation of cancer cells. Therefore, combination treatment therapy that targets both the CSC subsets and the differentiated cancer cells represents an ideal therapeutic regimen to attain complete eradication of cancer. Collectively, findings presented in this study provide evidence to show the clinical relevance, functional significance, and therapeutic implication of both endogenous and secretory ANXA3 in CD133$^+$ liver CSCs and HCC. We believe that ANXA3 can be used as a novel biomarker for the better detection of HCC and that targeting ANXA3 can be potentially developed as a novel treatment regime for this disease.

EXPERIMENTAL PROCEDURES

Cell lines, patient samples, reagents, plasmids, in vitro and in vivo assays, antibody production, microscopy, and statistical analyses are described in Supplemental Experimental Procedures.

ACCESSION NUMBERS

The GEO accession number for the RNA-seq data reported in this paper is GSE62905.

SUPPLEMENTAL INFORMATION

Supplemental Information includes Supplemental Experimental Procedures, five figures, and four tables and can be found with this article online at http://dx.doi.org/10.1016/j.stemcr.2015.05.013.

AUTHOR CONTRIBUTIONS

M.T. and S.M. conceived the project. M.T., K.-Y.N., S.T.L., T.K.L., and S.M. performed the experiments and analyzed the data. M.T., T.-M.F., and C.-H.L. performed statistical analysis. J.W.Y. provided reagents for caveolin-1 studies. K.W.C. provided advice on histology. F.N. and B.-J.Z. provided help with sorting. C.M.L, K.M., X.-Y.G., Y.-F.Y., and D.X. obtained consent from patients and provided the clinical samples and patient information. M.T. and S.M. wrote the manuscript.

ACKNOWLEDGMENTS

We thank the Faculty Core Facility at the Faculty of Medicine, HKU for providing and maintaining the equipment needed for flow cytometry, sorting, animal imaging, and confocal microscopy. We also thank Yuen-Piu Chan and Pak-Shing Kwan for their assistance and help with statistical analysis. This study is supported by the RGC GRF (HKU_774513M, HKU_773412M) and CRF (C7027-14G), HMRF (12110792), the NSFC Science Fund for Young Scholars (81302171), and a Croucher Innovation Award (to S.M.). A patent application has been filed for the anti-ANXA3 mAb (US14/485,206).

Received: December 7, 2014
Revised: May 19, 2015
Accepted: May 21, 2015
Published: June 18, 2015

REFERENCES

Hagiwara, S., Kudo, M., Nagai, T., Inoue, T., Ueshima, K., Nishida, N., Watanabe, T., and Sakurai, T. (2012). Activation of JNK and high expression level of CD133 predict a poor response to sorafenib in hepatocellular carcinoma. Br. J. Cancer *106*, 1997–2003.

Haraguchi, N., Utsunomiya, T., Inoue, H., Tanaka, F., Mimori, K., Barnard, G.F., and Mori, M. (2006). Characterization of a side population of cancer cells from human gastrointestinal system. Stem Cells *24*, 506–513.

Harashima, M., Harada, K., Ito, Y., Hyuga, M., Seki, T., Ariga, T., Yamaguchi, T., and Niimi, S. (2008). Annexin A3 expression increases in hepatocytes and is regulated by hepatocyte growth factor in rat liver regeneration. J. Biochem. *143*, 537–545.

Jin, Y., Mao, J., Wang, H., Hou, Z., Ma, W., Zhang, J., Wang, B., Huang, Y., Zang, S., Tang, J., and Li, L. (2013). Enhanced tumorigenesis and lymphatic metastasis of CD133+ hepatocarcinoma ascites syngeneic cell lines mediated by JNK signaling pathway in vitro and in vivo. Biomed. Pharmacother. *67*, 337–345.

Köllermann, J., Schlomm, T., Bang, H., Schwall, G.P., von Eichel-Streiber, C., Simon, R., Schostak, M., Huland, H., Berg, W., Sauter, G., et al. (2008). Expression and prognostic relevance of annexin A3 in prostate cancer. Eur. Urol. *54*, 1314–1323.

Lee, T.K., Castilho, A., Cheung, V.C., Tang, K.H., Ma, S., and Ng, I.O. (2011). CD24(+) liver tumor-initiating cells drive self-renewal and tumor initiation through STAT3-mediated NANOG regulation. Cell Stem Cell *9*, 50–63.

Liu, Y.F., Xiao, Z.Q., Li, M.X., Li, M.Y., Zhang, P.F., Li, C., Li, F., Chen, Y.H., Yi, H., Yao, H.X., and Chen, Z.C. (2009). Quantitative proteome analysis reveals annexin A3 as a novel biomarker in lung adenocarcinoma. J. Pathol. *217*, 54–64.

Ma, S., Chan, K.W., Hu, L., Lee, T.K., Wo, J.Y., Ng, I.O., Zheng, B.J., and Guan, X.Y. (2007). Identification and characterization of tumorigenic liver cancer stem/progenitor cells. Gastroenterology *132*, 2542–2556.

Ma, S., Lee, T.K., Zheng, B.J., Chan, K.W., and Guan, X.Y. (2008). CD133+ HCC cancer stem cells confer chemoresistance by preferential expression of the Akt/PKB survival pathway. Oncogene *27*, 1749–1758.

Ma, S., Tang, K.H., Chan, Y.P., Lee, T.K., Kwan, P.S., Castilho, A., Ng, I., Man, K., Wong, N., To, K.F., et al. (2010). miR-130b Promotes CD133(+) liver tumor-initiating cell growth and self-renewal via tumor protein 53-induced nuclear protein 1. Cell Stem Cell *7*, 694–707.

Pan, Q.Z., Pan, K., Weng, D.S., Zhao, J.J., Zhang, X.F., Wang, D.D., Lv, L., Jiang, S.S., Zheng, H.X., and Xia, J.C. (2013). Annexin A3 promotes tumorigenesis and resistance to chemotherapy in hepatocellular carcinoma. Mol. Carcinog. Published online December 23, 2013. http://dx.doi.org/10.1002/mc.22126.

Pan, Q.Z., Pan, K., Wang, Q.J., Weng, D.S., Zhao, J.J., Zheng, H.X., Zhang, X.F., Jiang, S.S., Lv, L., Tang, Y., et al. (2015). Annexin A3 as a potential target for immunotherapy of liver cancer stem-like cells. Stem Cells *33*, 354–366.

Pardal, R., Clarke, M.F., and Morrison, S.J. (2003). Applying the principles of stem-cell biology to cancer. Nat. Rev. Cancer *3*, 895–902.

Park, J.E., Lee, D.H., Lee, J.A., Park, S.G., Kim, N.S., Park, B.C., and Cho, S. (2005). Annexin A3 is a potential angiogenic mediator. Biochem. Biophys. Res. Commun. *337*, 1283–1287.

Raynal, P., and Pollard, H.B. (1994). Annexins: the problem of assessing the biological role for a gene family of multifunctional calcium- and phospholipid-binding proteins. Biochim. Biophys. Acta *1197*, 63–93.

Schostak, M., Schwall, G.P., Poznanović, S., Groebe, K., Müller, M., Messinger, D., Miller, K., Krause, H., Pelzer, A., Horninger, W., et al. (2009). Annexin A3 in urine: a highly specific noninvasive marker for prostate cancer early detection. J. Urol. *181*, 343–353.

Tang, K.H., Ma, S., Lee, T.K., Chan, Y.P., Kwan, P.S., Tong, C.M., Ng, I.O., Man, K., To, K.F., Lai, P.B., et al. (2012). CD133(+) liver tumor-initiating cells promote tumor angiogenesis, growth, and self-renewal through neurotensin/interleukin-8/CXCL1 signaling. Hepatology *55*, 807–820.

Tong, S.W., Yang, Y.X., Hu, H.D., An, X., Ye, F., Hu, P., Ren, H., Li, S.L., and Zhang, D.Z. (2012). Proteomic investigation of 5-fluorouracil resistance in a human hepatocellular carcinoma cell line. J. Cell. Biochem. *113*, 1671–1680.

Tsai, S.T., Tsou, C.C., Mao, W.Y., Chang, W.C., Han, H.Y., Hsu, W.L., Li, C.L., Shen, C.N., and Chen, C.H. (2012). Label-free quantitative proteomics of CD133-positive liver cancer stem cells. Proteome Sci. *10*, 69.

Wu, N., Liu, S., Guo, C., Hou, Z., and Sun, M.Z. (2013). The role of annexin A3 playing in cancers. Clin. Transl. Oncol. *15*, 106–110.

Yamashita, T., Ji, J., Budhu, A., Forgues, M., Yang, W., Wang, H.Y., Jia, H., Ye, Q., Qin, L.X., Wauthier, E., et al. (2009). EpCAM-positive hepatocellular carcinoma cells are tumor-initiating cells with stem/progenitor cell features. Gastroenterology *136*, 1012–1024.

Yan, X., Yin, J., Yao, H., Mao, N., Yang, Y., and Pan, L. (2010). Increased expression of annexin A3 is a mechanism of platinum resistance in ovarian cancer. Cancer Res. *70*, 1616–1624.

Yin, J., Yan, X., Yao, X., Zhang, Y., Shan, Y., Mao, N., Yang, Y., and Pan, L. (2012). Secretion of annexin A3 from ovarian cancer cells and its association with platinum resistance in ovarian cancer patients. J. Cell. Mol. Med. *16*, 337–348.

Yoon, C.H., Kim, M.J., Kim, R.K., Lim, E.J., Choi, K.S., An, S., Hwang, S.G., Kang, S.G., Suh, Y., Park, M.J., and Lee, S.J. (2012). c-Jun N-terminal kinase has a pivotal role in the maintenance of self-renewal and tumorigenicity in glioma stem-like cells. Oncogene *31*, 4655–4666.

Stem Cell Reports, Volume *5*

Supplemental Information

ANXA3/JNK Signaling Promotes Self-Renewal and Tumor Growth, and Its Blockade Provides a Therapeutic Target for Hepatocellular Carcinoma

Man Tong, Tsun-Ming Fung, Steve T. Luk, Kai-Yu Ng, Terence K. Lee, Chi-Ho Lin, Judy W. Yam, Kwok Wah Chan, Fai Ng, Bo-Jian Zheng, Yun-Fei Yuan, Dan Xie, Chung-Mau Lo, Kwan Man, Xin-Yuan Guan, and Stephanie Ma

Supplemental Figures and Figure Legends

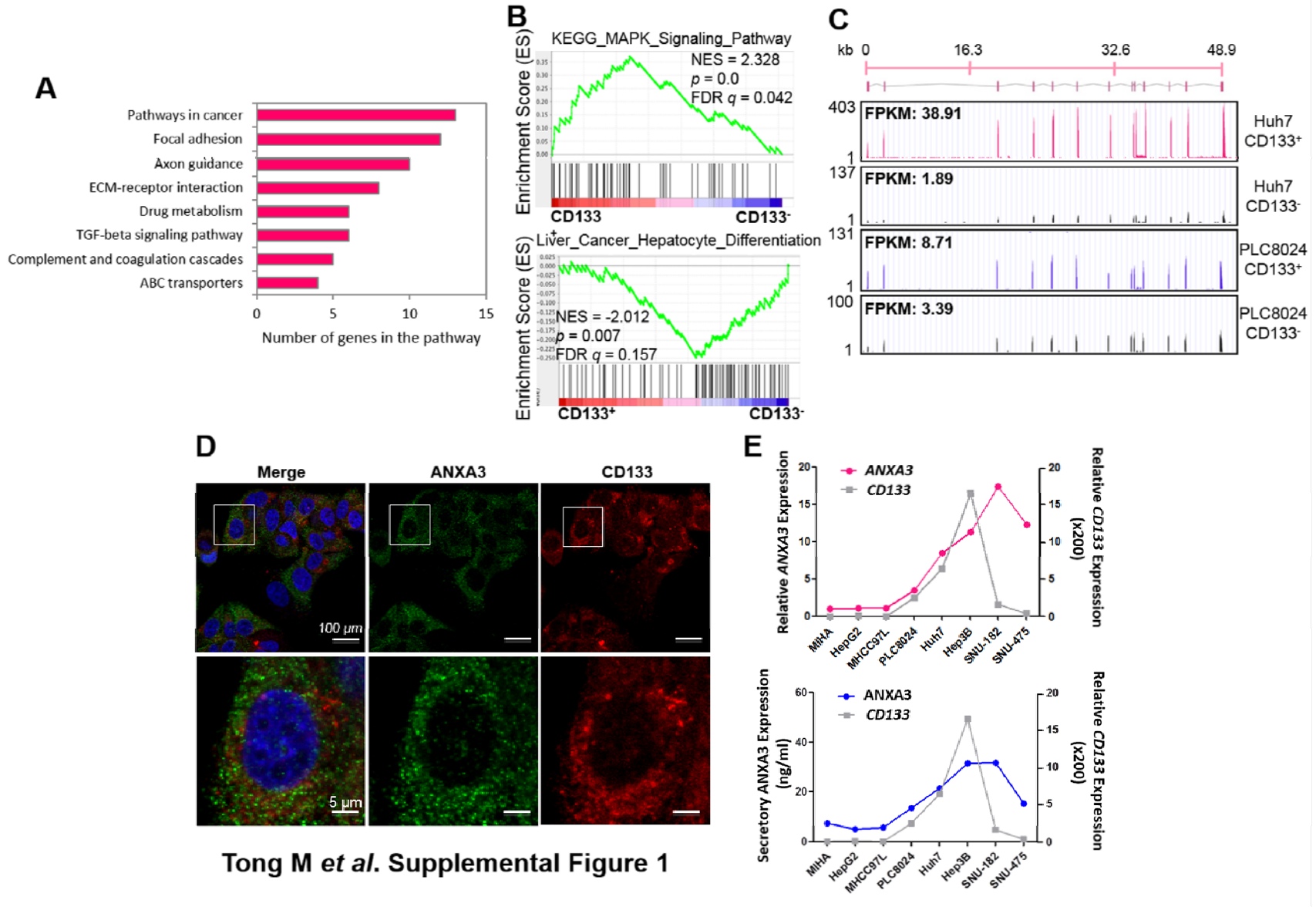

Tong M *et al*. Supplemental Figure 1

Supplemental Figure S1. Positive correlation between ANXA3 and CD133 in HCC. (Related to Figure 1) (**A**) Most significantly enriched pathways common between $CD133^+$ liver CSCs vs. $CD133^-$ non-CSC subsets isolated from Huh7 and PLC8024 HCC cells by DAVID bioinformatics analysis software. (**B**) GSEA comparison of differentially expressed genes in $CD133^+$ vs. $CD133^-$ subsets isolated from Huh7 and PLC8024 HCC cells identified enrichment of *MAPK* signaling in $CD133^+$ liver CSCs and hepatocyte differentiation in $CD133^-$ non-CSC subsets. NES, normalized enrichment score; FDR *q*, false discovery rate *q* value. (**C**) RNA-Seq read mapping to the University of California, Santa Cruz (UCSC) reference genome (hg19) of the *ANXA3* (NM_005139) gene. The absolute read counts for each sample are indicated on the *y*-axis. (**D**) Dual-color IF images of CD133 (red) and ANXA3 (green) in PLC8024 cells. Nuclei stained with DAPI (blue). Images shown of data from 3 independent experiments. (**E**) mRNA and secretory ANXA3 levels across a panel of liver cell lines as detected by qRT-PCR and ELISA, respectively, relative to CD133 expression.

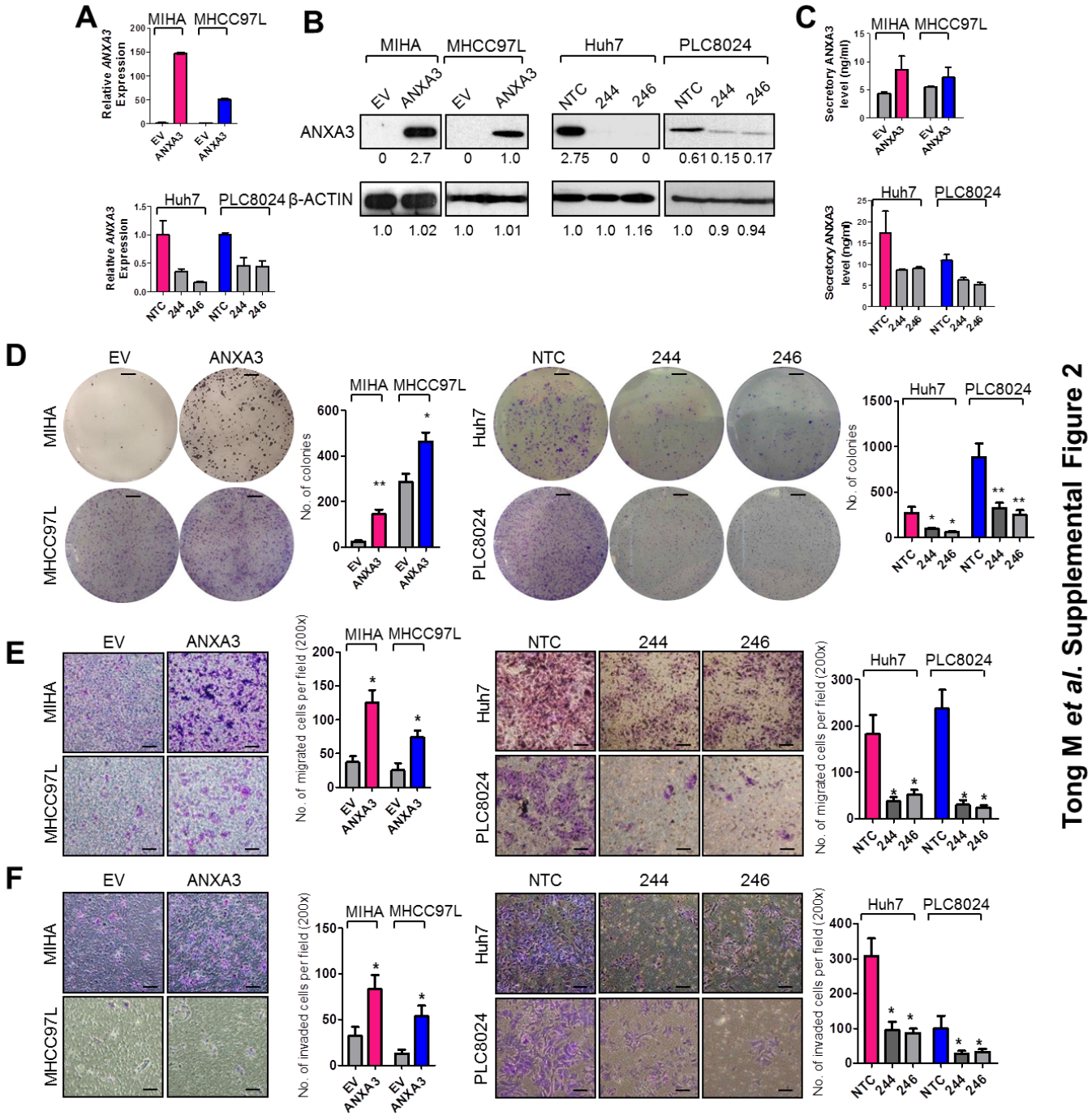

Tong M *et al.* Supplemental Figure 2

Supplemental Figure S2. Endogenous ANXA3 confers enhanced clonogenicity, migration and invasion abilities in HCC. (Related to Figures 2 and 3) (**A to C**) Validation of ANXA3 overexpression (MIHA and MHCC97L) and knockdown (Huh7 and PLC8024) at genomic levels by qPCR, endogenous proteomic levels by Western blot and secretory levels by ELISA. Error bars represent ±SD. Western blot images shown of data gathered from 3 independent experiments. (**D**) Quantification of colonies induced by the indicated stable cell lines. *p<0.05 and **p<0.01. Scale 5mm. Results represent mean ±SD from triplicate wells in 3 independent experiments. (**E and F**) Quantification of number of cells that migrated or invaded in the indicated stable cell lines. *p<0.05. Scale 100μm. Results represent mean ±SD from 3 independent experiments.

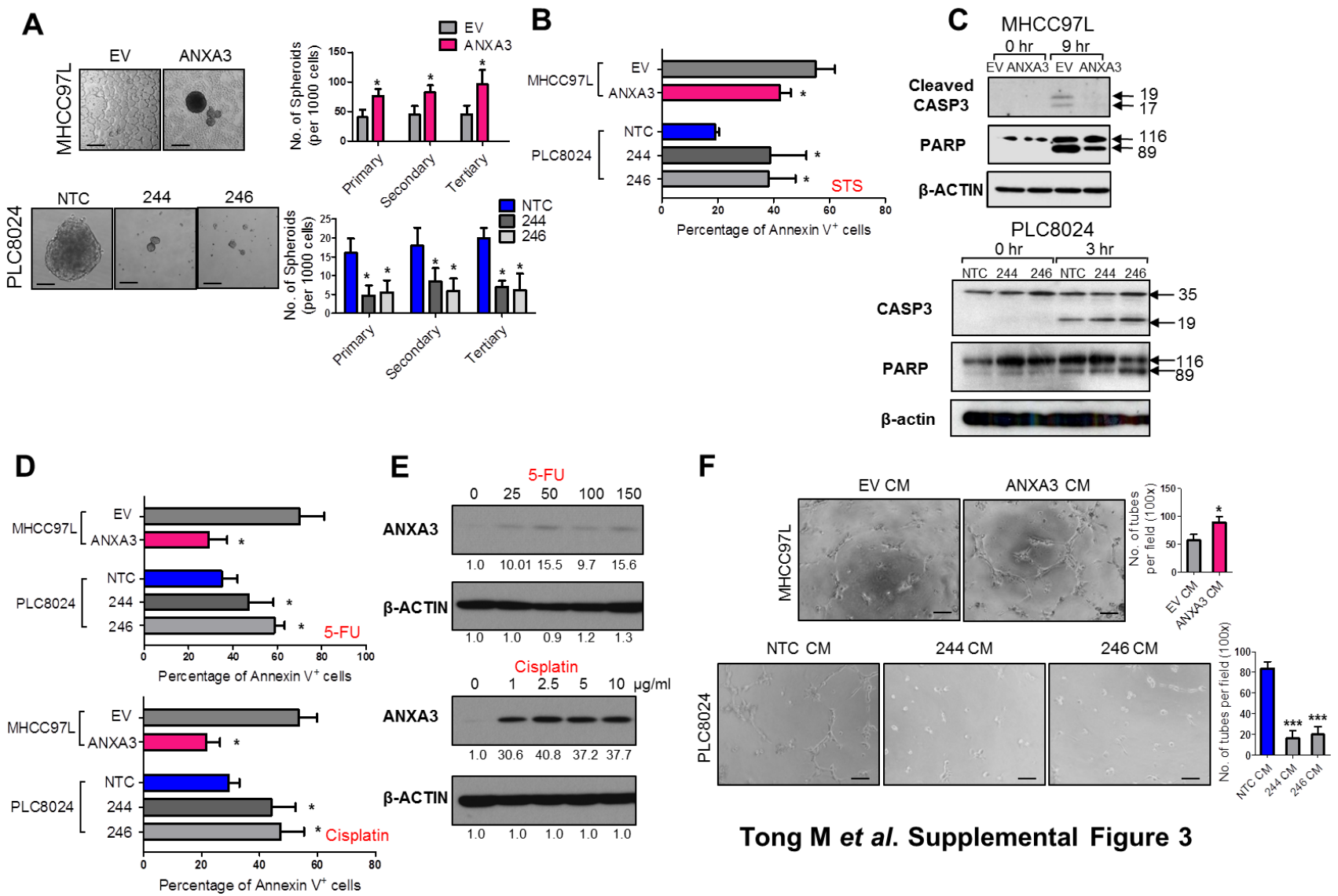

Tong M *et al.* Supplemental Figure 3

Supplemental Figure S3. Endogenous ANXA3 confers enhanced cancer and stem cell-like properties in HCC. (Related to Figures 2 and 3) (**A**) Quantification of primary, secondary and tertiary hepatospheres in HCC cells with ANXA3 stably expressed (MHCC97L EV and ANXA3 O/E) or repressed (PLC8024 NTC and ANXA3 knockdown clones 244 and 246). *p<0.05. Scale 100μm. Results represent mean ±SD of 12 replicates in 3 independent experiments. (**B**) Percentage of Annexin V positive cells in MHCC97L and PLC8024 cells with ANXA3 stably expressed and repressed, respectively, following STS treatment. Results represent mean ±SD of 3 independent experiments. (**C**) Western blot showing expression of total and cleaved forms of caspase 3 and PARP in the indicated stable cell lines after STS treatment for various time points. (**D**) Percentage of Annexin V positive cells in MHCC97L and PLC8024 cells with ANXA3 stably expressed and repressed, respectively, following treatment with chemotherapeutic drugs, 5-FU and cisplatin. Results represent mean ±SD of 3 independent experiments. (**E**) Western blot showing expression of ANXA3 protein in PLC8024 cells following treatment with increasing concentrations of 5-FU and cisplatin. (**F**) Quantification of capillary tubes formed by HUVEC cells following treatment with supernatant collected from MHCC97L and PLC8024 cells with ANXA3 stably expressed and repressed, respectively. *p<0.05 and ***p<0.001. Scale 100μm. Results represent mean ±SD of duplicate wells in 3 independent experiments. Representative images from 3 independent experiments unless otherwise specified.

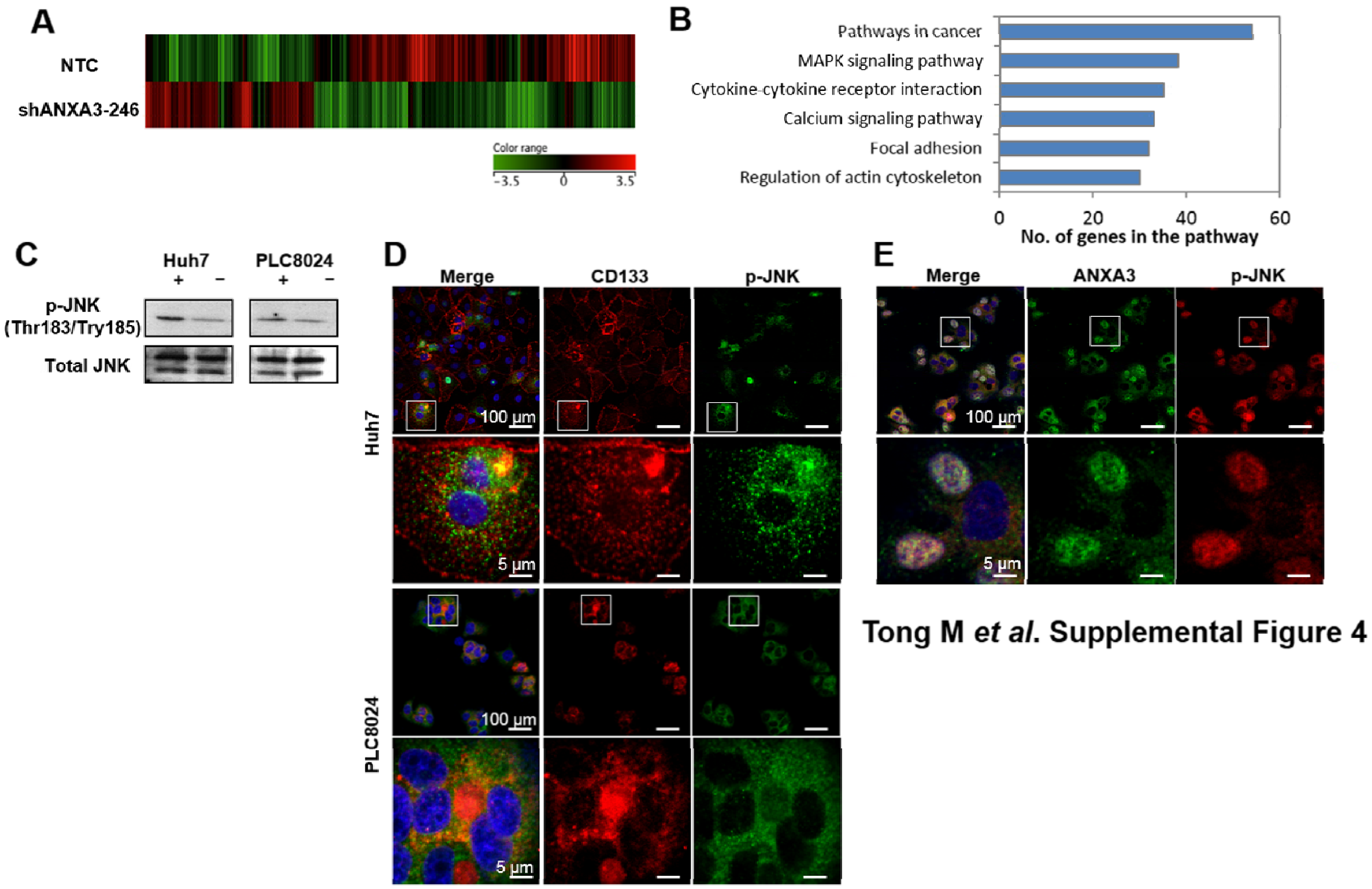

Tong M *et al*. Supplemental Figure 4

Supplemental Figure S4. ANXA3 and JNK are both preferentially overexpressed in the CD133$^+$ liver CSC subset. (Related to Figure 6) (**A**) Unique gene signatures of PLC8024 HCC cells with or without ANXA3 repressed, as shown by hierarchical cluster analysis (3-fold cutoff). Each cell in the matrix represents a particular expression level of genes, where red and green cells indicate high and low gene expression, respectively. (**B**) Most significantly enriched pathways associated with ANXA3 suppression in HCC by DAVID bioinformatics analysis software. (**C**) Western blot showing expression of p-JNK and total JNK in sorted CD133$^+$ and CD133$^-$ subsets from Huh7 and PLC8024. Please refer to Figure 1B for CD133, ANXA3 and β-ACTIN expression in CD133 sorted Huh7 and PLC8024. (**D**) Dual-color IF images of CD133 (red) and p-JNK (green) in Huh7 and PLC8024 cells. Nuclei stained with DAPI (blue). (**E**) Dual-color IF images of ANXA3 (green) and p-JNK (red) in PLC8024 cells. Nuclei stained with DAPI (blue). Representative images from 3 independent experiments for all results shown in this Figure.

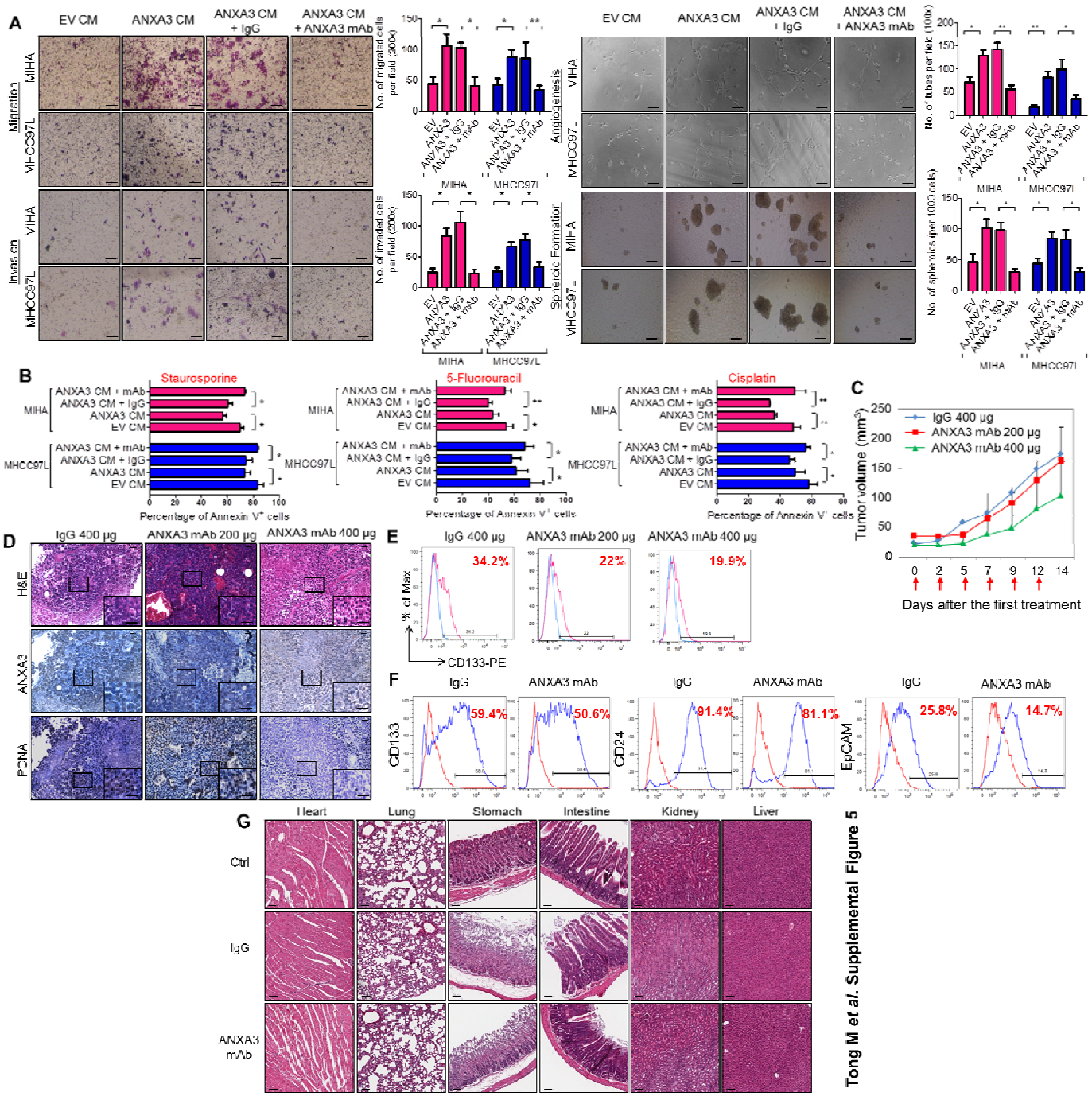

Tong M *et al.* Supplemental Figure 5

Supplemental Figure S5. ANXA3 ablation decreases the CD133$^+$ liver CSC subpopulation and attenuates tumor formation *in vivo*. (Related to Figure 7) (**A**) Left - Quantification of cells that migrated or invaded following treatment with conditioned medium collected from EV control or ANXA3 overexpressing cells and in the absence or presence of IgG control or ANXA3 monoclonal antibody. Results represent mean ±SD from 3 independent experiments. Right – Quantification of capillary tubes formed by HUVEC cells and spheroids formed following treatment with conditioned medium collected from EV control or ANXA3 overexpressing cells and in the absence or presence of IgG control or ANXA3 monoclonal antibody. *p<0.05 and **p<0.01. Scale 100μm. Results represent mean ±SD of duplicate wells in 3 independent experiments. (**B**) Percentage of Annexin V positive cells in MIHA and MHCC97L cells following treatment with conditioned medium collected from EV control or ANXA3 overexpressing cells and in the absence or presence of IgG control of ANXA3 monoclonal antibody. *p<0.05 and **p<0.01. Results represent mean ±SD of 3 independent experiments. (**C**) Graph showing the average tumor volumes of mice in each group along the course of treatment. Red arrows indicate the days when treatment was administered. Results represent mean ±SD of 5 mice from 1 independent experiment. (**D**) H&E images and IHC staining for expression of ANXA3 and PCNA in the resected xenograft tumors derived from the indicated treatment groups. Scale 200μm. (**E**) Flow cytometry analysis for expression of CD133 in the residual xenografts of the indicated treatment groups. (**F**) Flow cytometry analysis for expression of CD133, CD24 and EpCAM in Huh7 cells treated with IgG control or ANXA3 monoclonal antibody *in vitro*. (**G**) H&E images of major organs (heart, lung, stomach, intestine, kidney and liver) harvested from control untreated mice and mice treated with either IgG control or ANXA3 monoclonal antibody. Scale 100μm. Representative images from 3 independent experiments unless otherwise specified.

Supplemental Tables

Supplemental Table S1. Summary of RNA-Seq statistics and mapped reads for sorted CD133$^+$ and CD133$^-$ cells isolated from Huh7 and PLC8024. (Related to Figure 1)

Sample ID	No. of raw reads	No. of reads after filtering[1]	% of filtered reads	No. of reads mapped to reference genome[2]	% of mappable reads[3]
Huh7 CD133$^+$	65,441,262	62,913,906	96.14%	60,149,975	95.61%
Huh7 CD133$^-$	70,077,984	66,584,108	95.01%	63,376,438	95.18%
PLC8024 CD133$^+$	63,294,766	60,749,226	95.98%	58,238,955	95.87%
PLC8024 CD133$^-$	66,357,576	63,563,976	95.79%	60,878,505	95.78%
Average	**66,292,897**	**63,452,804**	**95.73%**	**60,660,968**	**95.61%**

[1]Raw reads were filtered with polymer track, adaptor sequences and rRNA repeating sequences.
[2]Sequencing reads were mapped to NCBI Build 37.1 (Genome Reference Consortium GRCh37 / hg19) with at most 2 mismatches.
[3]Percentage of mappable reads are the percentages of total filtered reads mapped to reference genome.

Supplemental Table S2. List of commonly differentially expressed genes in Huh7 and PLC8024 CD133$^+$ vs. CD133$^-$ identified by RNA-Seq profiling. p <0.05. (Related to Figure 1)

Gene[1]	Huh7 CD133$^+$ FPKM	Huh7 CD133$^-$ FPKM	Huh7 fold-change	PLC8024 CD133$^+$ FPKM	PLC8024 CD133$^-$ FPKM	PLC8024 fold-change
Up-regulated genes in the CD133$^+$ subset						
PROM1	71.24	1.76	40.40	31.01	5.75	5.39
ANXA3	***38.91***	***1.89***	***20.60***	***8.71***	***3.39***	***2.57***
CFTR	1.50	0.09	17.20	3.15	0.67	4.72
LRP2	13.17	0.78	16.81	11.00	4.01	2.75
BCO2	1.93	0.16	12.44	0.21	0.07	3.07
CCNJL	5.25	0.43	12.32	17.06	7.34	2.32
EDN1	***3.11***	***0.26***	***12.14***	***3.11***	***0.60***	***5.14***
ANKRD1	12.67	1.23	10.31	3.17	0.66	4.79
IL18	***24.39***	***2.42***	***10.08***	***16.72***	***7.96***	***2.10***
MTRNR2L6	8.78	1.00	8.81	8.25	2.83	2.91
THSD4	***1.81***	***0.21***	***8.44***	***0.08***	***0.03***	***2.77***
FSTL1	***2.59***	***0.35***	***7.47***	***0.50***	***0.21***	***2.34***
PRSS23	***6.77***	***0.91***	***7.43***	***14.39***	***2.61***	***5.52***
VIM	128.35	20.82	6.17	19.20	4.98	3.86
UBASH3B	0.96	0.18	5.45	7.84	2.41	3.25
DPP4	100.72	18.55	5.43	0.06	0.03	2.21
MOXD1	1.75	0.32	5.41	3.41	0.65	5.21
MTRNR2L10	3.39	0.65	5.23	3.98	0.56	7.08
SULT1E1	17.79	3.49	5.09	0.06	0.02	3.85
CTTNBP2	2.06	0.44	4.70	0.19	0.02	8.59
AOX1	4.73	1.01	4.69	0.06	0.01	10.38
TFPI2	***14.70***	***3.14***	***4.68***	***9.16***	***4.32***	***2.12***
CYR61	***7.32***	***2.24***	***3.27***	***30.80***	***6.42***	***4.80***
DNAH5	0.04	0.02	2.35	0.47	0.09	4.95
KCP	***0.67***	***0.29***	***2.35***	***0.04***	***0.01***	***3.22***
GJA1	149.41	65.00	2.30	100.28	14.13	7.10
THBS1	***2.89***	***1.27***	***2.27***	***9.90***	***1.75***	***5.64***
PGBD5	1.39	0.63	2.20	7.50	2.26	3.32
TMEM200A	2.93	1.36	2.16	1.94	0.41	4.73
SLC2A3	1.24	0.61	2.05	123.22	42.98	2.87
CDH2	45.28	22.36	2.03	0.56	0.08	6.81
Down-regulated genes in the CD133$^+$ subset						
ORM1	114.56	248.10	0.46	75.10	238.49	0.31
ORM2	56.88	125.16	0.45	21.10	63.62	0.33
AHSG	***69.28***	***174.14***	***0.40***	***1.12***	***3.99***	***0.28***
HAL	2.53	6.79	0.37	2.27	9.89	0.23
F5	***2.56***	***10.25***	***0.25***	***1.32***	***2.71***	***0.49***
PCSK9	***5.97***	***25.16***	***0.24***	***16.23***	***43.57***	***0.37***
NKX3-1	0.38	2.94	0.13	0.05	0.14	0.36

[1]Genes that encode for secretory proteins are denoted in red italics and in bold font.

Supplemental Table S3. Clinico-pathological correlation of endogenous ANXA3 expression in 83 HCC tissue samples. (Related to Figure 1)

Clinical Features	Total no. of cases[1]	Without *ANXA3* overexpression[2]	*ANXA3* overexpression[2]	*p* value
Gender				
Male	67	33 (49.3%)	34 (50.7%)	0.856
Female	15	7 (46.7%)	8 (53.3%)	
Age				
<50	45	19 (42.2%)	26 (57.8%)	0.19
≥50	37	21 (56.8%)	16 (43.2%)	
HBsAg				
Negative	9	3 (33.3%)	6 (66.7%)	0.288
Positive	71	37 (52.1%)	34 (47.9%)	
HCV antibody				
Negative	79	40 (50.6%)	39 (49.4%)	1
Positive	1	0 (0%)	1 (100%)	
Cirrhosis				
No / Mild	56	24 (42.9%)	32 (57.1%)	0.071
Moderate / Severe	23	15 (65.2%)	8 (34.8%)	
No. of nodules				
Single	68	35 (51.5%)	33 (48.5%)	0.39
Multiple	13	5 (38.5%)	8 (61.5%)	
Tumor size				
<5 cm	76	38 (50%)	38 (50%)	1
≥5 cm	5	2 (40%)	3 (60%)	
Vascular invasion				
Negative	71	37 (52.1%)	34 (47.9%)	0.312
Positive	10	3 (30%)	7 (70%)	
Encapsulation				
No / Incomplete	46	21 (45.7%)	25 (54.3%)	0.441
Complete	35	19 (54.3%)	16 (45.7%)	
Adjacent organ invasion				
Negative	70	34 (48.6%)	36 (51.4%)	0.927
Positive	12	6 (50%)	6 (50%)	
HCC stage				
Stage I / II	60	34 (56.7%)	26 (43.3%)	***0.027**
Stage III	21	6 (28.6%)	15 (71.4%)	
Differentiation				
Poor	38	17 (44.7%)	21 (55.3%)	0.263
Moderate	35	17 (48.6%)	18 (51.4%)	
Well	6	5 (83.3%)	1 (16.6%)	
Satellite				
Negative	56	26 (46.4%)	30 (53.6%)	0.473
Positive	14	8 (57.1%)	6 (42.9%)	

[1]Clinical data was not available for some patients; statistics were calculated based on available data only.
[2]HCC specimens demonstrating a fold-change increase of over 1.5 as compared to matched non-tumor samples are classified as ANXA3 overexpression.

Supplemental Table S4. Clinico-pathological correlation of secretory ANXA3 levels in 60 HCC serum samples. (Related to Figure 1)

Clinical Features	Total no. of cases[1]	Low ANXA3[2]	High ANXA3[2]	*p* value
Gender				
Male	48	19 (39.6%)	29 (60.4%)	***0.011**
Female	11	9 (81.8%)	2 (18.2%)	
Age				
<59	29	16 (55.2%)	13 (44.8%)	0.243
≥59	30	12 (40.0%)	18 (60%)	
Family history				
Negative	50	21 (42.0%)	29 (58.0%)	0.071
Positive	9	7 (77.8%)	2 (22.2%)	
AFP elevation				
Negative	45	19 (42.2%)	26 (57.8%)	0.149
Positive	14	9 (64.3%)	5 (35.7%)	
HBeAg				
Negative	31	20 (64.5%)	11 (35.5%)	0.111
Positive	13	5 (38.5%)	8 (61.5%)	
HbsAg				
Negative	51	25 (49%)	26 (51%)	1
Positive	7	3 (42.9%)	4 (57.1%)	
HCV carrier				
Negative	57	27 (47.4%)	30 (52.6%)	1
Positive	2	1 (50%)	1 (50%)	
No. of nodules				
Single	29	18 (62.1%)	11 (37.9%)	***0.036**
Multiple	29	10 (34.5%)	19 (65.5%)	
Tumor size				
<5 cm	49	27 (55.1%)	22 (44.9%)	***0.005**
≥5 cm	8	0 (0%)	8 (100%)	
HCC stage				
Stage I / II	29	21 (72.4%)	8 (27.6%)	***<0.001**
Stage III / VI	30	7 (23.3%)	23 (76.7%)	
Previous malignancy				
Negative	55	28 (50.9%)	27 (49.1%)	0.114
Positive	4	0 (0%)	4 (100%)	

[1]Clinical data was not available for some patients; statistics were calculated based on available data only.
[2]HCC serum samples are classified into low / high ANXA3 based on the median serum ANXA3 level among all cases.

Supplemental Experimental Procedures

Cell lines. Human HCC cell lines, Hep3B, SNU-182, SNU-475 and HepG2, were purchased from American Type Culture Collect (ATCC). HCC cell line, PLC8024, was obtained from the Institute of Virology, Chinese Academy of Medical Sciences, Beijing, China. HCC cell line, Huh7, was provided by Dr. H. Nakabayashi, Hokkaido University School of Medicine, Japan. Immortalized normal liver cell line, MIHA, was provided by Dr. J. R. Chowdhury, Albert Einstein College of Medicine, New York. Metastatic human HCC cell line, MHCC97L, was obtained from the Liver Cancer Institute, Fudan University, Shanghai, China. Chinese hamster ovary cell line CHO-K1 was purchased from ATCC. 293FT cells used for lentiviral transduction and human umbilical vein endothelial cells (HUVEC) were purchased from Invitrogen. All cell lines used in this study were regularly authenticated by morphological observation and tested for absence of Mycoplasma contamination (MycoAlert, Lonza).

Patient samples. Primary human HCC and adjacent non-tumor liver tissue samples were obtained from 83 patients undergoing surgical resection at either the Queen Mary Hospital in Hong Kong or the Sun Yat-Sen University Cancer Centre in Guangzhou, China. Venous blood samples were collected from 60 HCC patients, 20 HBV carriers, 20 patients with liver cirrhosis and 32 normal control individuals. Tissue samples were collected from patients who had not received any previous local or systemic treatment prior to operation. Venous blood samples were collected from HCC patients before any therapeutic procedures were performed. Use of human samples was approved by the committee for ethical review of research involving human subjects at the Queen Mary Hospital or Sun Yat-Sen University Cancer Centre.

Reagents, kits and plasmids. Serum ANXA3 and secretory ANXA3 in conditioned media was quantified using the Human ANXA3 ELISA Kit (Cusabio Biotech). Serum AFP was quantified using the AFP ELISA kit (Aviva Systems Biology). The human recombinant ANXA3 protein used for functional studies was purchased from Origene. JNK inhibitor SP600125 was purchased from Calbiochem. JNK activity was determined by KinaseSTAR™ JNK Activity Assay Kit (BioVision). A FLAG-tagged ANXA3 sequence was cloned into pcDNA6B/myc-His B vector (Invitrogen) in between EcoRI and XhoI or into pSNAP-tag (T7)-2 vector (New England Biolabs) in between EcoRI and HindIII.

Flow cytometry and cell sorting. Flow cytometry analysis or flow cytometry cell sorting was conducted using PE-conjugated mouse anti-human CD133 (Miltenyi Biotec), PE-conjugated mouse anti-human CD24, FITC-conjugated mouse anti-human EpCAM (BD Biosciences) or their respective

isotype controls. Samples were analyzed and sorted on BD FACSCanto II and FACSAria I, respectively (BD Biosciences) with data analyzed by FlowJo (Tree Star Inc.). For analysis and cell sorting of freshly resected clinical samples and xenograft tumors, tissue samples would first be digested with a mixture of Liberase, DNase I (Roche) and complete DMEM/F12 medium (Invitrogen) on a Miltenyi Biotec gentleMACS dissociator (Miltenyi Biotec), passed through 100 μM strainers with single cells stained with 7-AAD (BD Biosciences) to exclude dead cells. Detailed protocols described in our previous studies (Ma et al., 2010; Tang et al., 2012).

RNA sequencing. RNA sequencing was performed as a service at the Centre for Genomic Sciences of The University of Hong Kong. Expression levels were tabulated in accordance with the number of exon reads to the length of exons within that gene and per million mapped reads (FPKM).

Quantitative real-time PCR. Total RNA was extracted using RNA-IsoPlus (Takara) and cDNA was synthesized by PrimeScript RT Master Mix (Takara). qPCR was performed with SYBR Green PCR Master Mix (Applied Biosystems) and the following primers *ANXA3*: F (5'-GCAGGAGGAAGGGGTGCGGT-3'); R (5'-TCCAAAGCGCGGTGGGGGAA-3') and *β-ACTIN*: F (5'- CATCCACGAAACTACCTTCAACTCC-3'); R (5'- GAGCCGCCGATCCACACG-3') on an ABI Prism 7900 System (Applied Biosystems) with data analyzed using the ABI SDS v2.3 software (Applied Biosystems). Relative expression differences were calculated using the $2^{-\Delta\Delta Ct}$ method.

Western blot and immunoprecipitation. Protein lysates were quantified and resolved on a SDS-PAGE gel, transferred onto a PVDF membrane (Millipore) and immunoblotted with a primary antibody, followed by incubation with a secondary antibody. Antibody signal was detected using an enhanced chemiluminescence system (GE Healthcare). The following antibodies were used: ANXA3 (1:800, Abcam, ab33068), CD133 (1:800, Miltenyi Biotec, 130-092-395), CAV1 (1:5000, BD Biosciences, 610060), caspase 3 (1:1000, Cell Signaling Technology, 9662), PARP (1:1000, Cell Signaling Technology, 9542), p-JNK1 (Thr183/Tyr185) (1:2000, Cell Signaling Technology, 9255), total JNK (1:1000, Cell Signaling Technology, 9252), p-MKK4 (Ser257/Thr261) (1:1000, Cell Signaling Technology, 9156), C-MYC (1:500, Invitrogen, 13-2500), p21 (1:1000, Cell Signaling Technology, 2946), FLAG (1:5000, Sigma-Aldrich, F3165), β-ACTIN (1:5000, Sigma-Aldrich, A5316) and GAPDH (1:1000, Cell Signaling Technology, 5174). Immunoprecipitation was performed with anti-FLAG M2 affinity gel (Sigma-Aldrich). ImageJ software was used for densitometric analyses of western blot bands, and the quantification results were normalized to the loading control.

Luciferase reporter assay. A luciferase reporter construct consisting of the consensus sequence of AP-1 binding site was co-transfected with a Renilla luciferase reporter construct into cells plated on 96-well using Lipofectamine 2000 (Invitrogen). 48 hours after transfection, reporter activity was determined using the Dual-Glo Luciferase Assay Kit (Promega) according to the manufacturer's protocol and measured with plate reader (Victor^3 1420 Multilabel Plate Counter) (Perkin Elmer). Experiments were performed in triplicates.

Lentiviral transduction. ANXA3-specific shRNA expression vectors (NM_0005139), CAV1-specific shRNA expression vectors (NM_001753) and the scrambled shRNA non-target control (NTC) were purchased from Sigma-Aldrich. Sequences of the two shRNAs directed against ANXA3 are as follows: clone ID TRCN0000056244 (CCGGCCAGATCAGAAATTGACCTTTCTCGAGAAAGGTCAATTTCTGATCTGGTTTTTG) and clone ID TRCN0000056246 (CCGGGTAAGAGATTATCCAGACTTTCTCGAGAAAGTCTGGATAATCTCTTACTTTTTG). Sequences of the two shRNAs directed against CAV1 are as follows: clone ID TRCN0000008001 (CCGGGACCCTAAACACCTCAACGATCTCGAGATCGTTGAGGTGTTTAGGGTCTTTTT) and clone ID TRCN0000008002 (CCGGGACGTGGTCAAGATTGACTTTCTCGAGAAAGTCAATCTTGACCACGTCTTTTT). Sequence of NTC is (CCGGCAACAAGATGAAGAGCACAACTCGAGTTGGTGCTCTTCATCTTGTTGTTTTT). Sequences were transfected into 293FT cells and packaged using MISSION Lentiviral Packaging Mix (Sigma-Aldrich). ANXA3 lentiviral overexpression or empty vector control plasmids were purchased from GeneCopoeia. CAV1 open reading frame sequence was cloned into pLenti6/V5-D-TOPO-Myc vector. Sequences were transfected into 293FT cells and packaged using Lenti-Pac HIV expression packaging mix (GeneCopoeia) or Viral Power packaging mix (Invitrogen). Virus-containing supernatants were collected for subsequent transduction to establish cells with ANXA3 or CAV1 stably repressed or overexpressed. Puromycin and blasticidin were used to select for cells with stable overexpression of ANXA3 and CAV1, respectively.

Immunohistochemistry. Slides were heated for antigen retrieval in 10 mM sodium citrate (pH 6.0). Endogenous peroxidase activity was inhibited with 3% hydrogen peroxide. Sections were subsequently incubated with mouse anti-human PCNA (Santa Cruz) or mouse anti-human ANXA3 (Origene). Reaction was developed with DAB+ Substrate-Chromogen System (Dako). Slides were counterstained with Mayer's hematoxylin.

Immunofluorescence and confocal microscopy. Cells were fixed with 4% paraformaldehyde, permeabilized with 0.1% Triton X (Sigma), blocked with normal goat serum and incubated with PE-

conjugated mouse anti-human CD133 (Miltenyi Biotec), rabbit anti-human ANXA3 or rabbit anti-human phospho-JNK (Thr183/Tyr185) (Cell Signaling Technology), followed by Alexa-Fluor conjugated secondary antibody, where appropriate. Cells were counterstained with anti-fade DAPI (Invitrogen) and visualized by fluorescent confocal microscope (Carl Zeiss LSM 700). For confocal imaging analysis of ANXA3 internalization, cells were labeled with Vybrant CFDA SE Cell Tracer Kit (Invitrogen). SNAP-tagged ANXA3 proteins labeled with SNAP-Surface Alexa Fluor 546 substrate (New England Biolabs) were co-cultured with CFDA-dye labeled cells for 3 hours. Cells were fixed with 1% paraformaldehyde and visualized by fluorescent confocal microscope (Perkin Elmer).

Hepatosphere-forming and self-renewal assay. Single cells were cultured in 300 µl of serum-free DMEM/F12 medium (Invitrogen) supplemented with 20 ng/ml human recombinant epidermal growth factor (Sigma-Aldrich), 10 ng/ml human recombinant basic fibroblast growth factor (Sigma-Aldrich), 4 µg/ml insulin (Sigma-Aldrich), B27 (1:50; Invitrogen), 500 U/ml penicillin, 500 µg/ml streptomycin (Invitrogen) and 1% methylcellulose (Sigma-Aldrich). Cells were cultured in suspension in poly-HEMA-coated 24-well plates. Cells were replenished with 30 µl of supplemented medium every second day. To propagate spheres *in vitro*, spheres were collected by gentle centrifugation and dissociated to single cells using TrypLE Express (Invitrogen). Following dissociation, trypsin inhibitor (Invitrogen) was used to neutralize the reaction, and the cells were cultured to generate the next generation of spheres.

Colony formation assay. $1x10^3$ cells were seeded in a 6-well plate and cultured in complete medium for 2 weeks. Surviving colonies (>50 cells per colony) were counted and stained with crystal violet (Sigma-Aldrich).

Cell motility and invasion assays. Migration and invasion assays were conducted in 24-well Millicell hanging inserts (Millipore) and 24-well BioCoat Matrigel Invasion Chambers (BD Biosciences), respectively. Cells re-suspended in serum free DMEM were added to the top chamber and medium supplemented with 10% FBS was added to the bottom chamber as a chemoattractant. After 48 hrs of incubation at 37°C, cells that migrated or invaded through the membrane (migration) or Matrigel (invasion) were fixed and stained with crystal violet (Sigma-Aldrich). The number of cells was counted in 3 random fields under 20x objective lens and imaged using SPOT imaging software (Nikon).

Annexin V apoptosis assay. Cells were treated with either 1 µg/mL STS for 6-16 hrs or with various concentrations of chemotherapeutic drugs, 5-FU and cisplatin (Huh7 with 150 mg/mL 5-FU or 1

mg/mL cisplatin and PLC8024 with 75 mg/mL 5-FU or 2 mg/mL cisplatin) for 48 hrs. Following treatment, cells were harvested and stained with propidium iodide (PI) and FITC-conjugated Annexin V as provided by the Annexin V-FLUOS Staining Kit (Roche). Samples were analyzed on BD FACSCanto II (BD Biosciences) with data analyzed by FlowJo (Tree Star Inc.).

Capillary tube formation assay in HUVECs. Cells were cultured in 6-well plates in complete medium, with culture medium replaced with serum free medium after 24 hrs. Conditioned medium was collected and filtered after incubation for a further 24 hrs. HUVECs were co-cultured with conditioned medium for 24 hrs. Capillary tube formation assays were then conducted on BD Matrigel Basement Membrane Matrix (BD Biosciences). The number of capillary tubes formed was counted in 3 random fields under a 20x objective lens and imaged using SPOT imaging software. Specifically, the formation of 1 capillary tube was defined as a connection between 2 cells.

Animal studies. The study protocol was approved by and performed in accordance with the Committee of the Use of Live Animals in Teaching and Research at The University of Hong Kong. Tumorigenicity was determined by subcutaneous injection into the flank of 4-to-5 week old male BALB/C nude or NOD/SCID mice. Tumor-initiating and self-renewal abilities were investigated by limiting dilution and serial transplantation assays. 4-to-6 week old male NOD/SCID mice were injected subcutaneously with either 5,000 or 10,000 cells. Tumor incidence and tumor latency were recorded. Established xenografts were harvested and dissociated for subsequence passage to secondary mouse recipients. After tumors were detected, tumor sizes were measured every 3 days by calipers and tumor volumes were calculated as volume (cm^3) = L x W^2 x 0.5 with L and W representing the largest and smallest diameters, respectively. Tumors formed were harvested for histological analysis. Metastasis was assessed by orthotopically injecting into the liver of 6 week old BALB/C nude mice to observe for lung metastasis. Specifically, luciferase-labeled cells were injected into the left lobes of the livers of BALB/C nude mice. Six weeks after implantation, mice were administered with 100 mg/kg D-luciferin via peritoneal injection 5 mins before bioluminescent imaging (IVIS™ 100 Imaging System, Xenogen). Livers were harvested for ex-vivo imaging and histological analysis. Animals that were injected with tumor cells but showed no sign of tumor burden were generally terminated six months after tumor cell inoculation, and animals were opened up at the injection sites to confirm that there was no tumor development.

Microarray expression analysis. RNA was assayed on the Affymetrix microarray platform with the Human Genome U133 Plus 2.0 GeneChips and analyzed using MicroArray Suite 5 (MAS5) method with

GeneSpring GX v.12 (Agilent). Experiments were carried out as a service at the Centre for Genomic Sciences of The University of Hong Kong. Pathway enrichment analyses on the differentially expressed genes were conducted using the web resource from The Database for Annotation, Visualization and Integrated Discovery (DAVID) version 6.7 (NIH) and GeneGo Metacore (Thomson Reuters).

ANXA3 monoclonal antibody production. Mouse anti-human ANXA3 monoclonal antibody (that recognizes the epitope peptides ENRWGTDEDK) was synthesized by AbMart, Shanghai, China.

Statistical analysis. Statistical analyses were performed using GraphPad Prism 5.0 (GraphPad Software, Inc.) and SPSS version 21.0 (IBM). Independent Student's *t*-test was used to compare the mean value of two groups. Clinico-pathological significance in clinical samples was evaluated by Fisher's exact test and independent Student's *t*-test for categorical data and continuous data, respectively. ROC analysis was performed using ROC-kit (GUI version 1.0.1, ROC libraries 1.0.3) developed by The University of Chicago. Statistical significance was defined as $p \leq 0.05$.